Title	Driven cast-in-situ pile capacity: insights from dynamic and static load testing
Author(s)	Flynn, Kevin N.; McCabe, Bryan A.
Publication Date	2021-02-11
Publication Information	Flynn, Kevin N., & McCabe, Bryan A. (2021). Driven cast-in-situ pile capacity: insights from dynamic and static load testing. Canadian Geotechnical Journal, 58(12), 1870-1883. doi:10.1139/cgj-2020-0630
Publisher	Canadian Science Publishing
Link to publisher's version	https://doi.org/10.1139/cgj-2020-0630
Item record	http://hdl.handle.net/10379/17131
DOI	http://dx.doi.org/10.1139/cgj-2020-0630

TITLE

Driven cast-in-situ pile capacity: insights from dynamic and static load testing

AUTHORS

Kevin N. Flynn[1]

Bryan A. McCabe[2]*

AFFILIATIONS

[1]Principal Geotechnical Engineer, AGL Consulting, Sandyford, Dublin 18, Ireland

[2]Senior Lecturer, School of Engineering, National University of Ireland, Galway, Ireland

*Corresponding author

Email: bryan.mccabe@nuigalway.ie

Telephone: +353-91-492021

ABSTRACT

Driven cast-in-situ (DCIS) piles are classified as large displacement piles. However, the use of an oversized driving shoe introduces additional complexities influencing shaft resistance mobilisation, over and above those applicable to preformed displacement piles. Therefore, several design codes restrict the magnitude of shaft resistance in DCIS pile design. In this paper, a series of dynamic load tests was performed on the temporary steel driving tubes during DCIS pile installation at three UK sites. The instrumented piles were subsequently subjected to maintained compression load tests to failure. The mobilised shear stresses inferred from the dynamic tests during driving were two to five times smaller than those on the as-constructed piles during maintained load testing. This was attributed to soil loosening along the tube shaft arising from the oversized base shoe. Nevertheless, the radial stress reductions appear to be reversible by the freshly-cast concrete fluid pressures which provide lower-bound estimates of radial total stress inferred from the measured shear stresses during static loading. This recovery in shaft resistance is not recognised in some European design practices, resulting in conservative design lengths. Whilst the shaft resistance of DCIS piles was underpredicted by the dynamic load tests, reasonable estimates of base resistance were obtained.

KEY WORDS: Driven cast-in-situ; dynamic load tests; static load tests; instrumented piles

WORD COUNT: 6846

INTRODUCTION

Driven cast-in-situ (DCIS) piles are typically classified as large displacement piles in European practice (e.g. BSI, 2015; DDG, 2013; NBN, 2014; NEN, 2019), despite sharing aspects of their construction with replacement piles (Flynn and McCabe 2016). As illustrated in Figure 1, the installation process involves driving a hollow steel tube to the required depth (or set) using an impact hammer. The tube is fitted with a sacrificial circular steel plate (driving shoe) at its base to prevent ingress of soil and water during driving; the diameter of this plate usually exceeds that of the tube with the purpose of reducing installation shaft resistance. Once driving is complete, the tube is filled with high slump concrete before being withdrawn. The reinforcement is typically inserted into the tube prior to casting; alternatively, it may be plunged into the wet concrete after removal of the tube.

While DCIS piles have been shown by Flynn and McCabe (2016, 2021) to behave in a similar manner to traditional preformed piles (i.e. precast concrete and closed-ended steel piles) when installed in coarse-grained strata, the DCIS pile construction process introduces additional complexities influencing the mobilisation of shaft resistance, over and above those applicable to traditional preformed displacement piles. These factors, discussed in detail by Flynn and McCabe (2021), include the possibility of soil loosening after the passage of the oversized driving shoe, the possibility of friction fatigue during driving (defined as the reduction in radial stress due to cyclic loading), changes in radial stresses following casting and subsequent curing, and increases in radial stresses during loading due to enhanced dilation resulting from the rough soil-pile interface created by in-situ concreting. Unfortunately, the absence of suitable instrumentation that can withstand the in-situ concreting process prevents a direct assessment of the changes in stress state at the pile-soil interface during these processes.

It is assumed by some practitioners that the reduced shaft resistance during installation, resulting from the use of an oversized driving shoe, prevails once the pile is constructed. For example, the Belgian annex to EC7 (NBN, 2014; Huybrechts et al. 2016) does not permit shaft resistance to be considered when an oversized shoe (defined as a diameter at least 50mm greater than diameter of the installation tube) is deployed; therefore, DCIS piles must be designed as fully end-bearing piles, unless the shaft resistance is validated by instrumented pile tests. Furthermore, the authors have observed a tendency in some DCIS piling projects for the design resistance to be verified using dynamic testing performed on the tube during installation (and prior to concreting) only, forsaking traditional static testing. While such a practice is somewhat motivated by the reliable predictions of static pile resistance obtained by dynamic load testing during installation and restrike of traditional preformed displacement piles (Likins and Rausche, 2004), as well as reduced costs (by omitting static load testing) and programme constraints, it inherently assumes that the capacity of tube during installation is representative of the final (post-construction) pile behaviour. This practice may be reinforced, at least to some extent, by the use of a design value for the coefficient of earth pressure at failure of $K_f = 1$ recommended by Fleming et al. (2008) for DCIS pile shafts, which has been shown by Flynn and McCabe (2021) to be overly conservative. The assumption that the process of tube installation governs the performance of the constructed pile, which has significant implications for the efficiency of DCIS pile designs, has not been formally challenged to date.

In this paper, dynamic load tests during installation and standard static load tests on DCIS piles are compared for three sites in the United Kingdom. Dynamic testing was initially performed on the steel installation tubes during driving to determine the mobilised resistances on the external shaft of the tubes, as well as those on the sacrificial driving shoe at the base. Following casting and an appropriate curing period, the same test piles were loaded to failure under maintained compression loads. The reinforcement cage of each test pile was instrumented with several levels of vibrating wire strain gauges to enable assessment of the shaft and base resistances during maintained loading. The capacities inferred from the static and dynamic load tests were compared to provide an insight into the installation process and its subsequent influence on DCIS pile behaviour. The arguments presented are supported by the results of dynamic pile tests on other displacement pile types at two of the sites.

BACKGROUND

The total resistance of a closed-ended pile under compression load Q_t comprises the shaft resistance Q_s and the base resistance Q_b, as given in Equation 1, assuming that the pile weight is insignificant:

$$Q_t = Q_s + Q_t = \tau_s A_s + q_b A_b \qquad \text{Eqn. 1}$$

where τ_s is the shear stress, A_s is the external shaft area (= πD_s, where D_s = pile shaft diameter), q_b is the base pressure and A_b (= $\pi D_b^2/4$, where D_b = pile base diameter) is the cross-sectional area at the base of the pile. Whilst the definition of pile failure remains contentious (Fellenius, 2020), the total resistance corresponding to a pile head displacement equivalent to 10% of the pile diameter is specified by Eurocode 7 (CEN, 2004).

Shear resistance

The ultimate shear stress τ_{sf} mobilised in granular soil is traditionally expressed using the following equation, based on conventional earth pressure theory:

$$\tau_{sf} = K_f \, \sigma'_{v0} \tan \delta_f \qquad \text{Eqn. 2}$$

where K_f is the lateral earth pressure coefficient at failure, σ'_{v0} is the vertical effective stress and δ_f is the interface friction angle at failure. Using a high-instrumented closed-ended steel pile known as the Imperial College Pile (ICP), Lehane et al. (1993) demonstrated that τ_{sf} for displacement piles in granular soil obeys the Coulomb failure criterion:

$$\tau_{\mathrm{sf}} = \sigma'_{\mathrm{rf}} \tan\delta_{\mathrm{f}} = \left(\sigma'_{\mathrm{rc}} + \Delta\sigma'_{\mathrm{rd}}\right)\tan\delta_{\mathrm{cv}} \qquad \text{Eqn. 3}$$

where σ'_{rf} is the radial effective stress at failure, σ'_{rc} is the radial effective stress after installation and equalisation, $\Delta\sigma'_{\mathrm{rd}}$ is the change in radial effective stress due to interface dilation during loading and δ_{cv} is the constant-volume interface friction angle (which is typically assumed to be equivalent to the constant-volume soil friction angle ϕ'_{cv} for cast-in-situ piles).

A series of instrumented DCIS pile tests in granular soil by Flynn (2014) and Flynn and McCabe (2016, 2021) demonstrated that the shaft resistance of DCIS piles in coarse-grained soils were comparable to traditional preformed piles. Whilst the normalised shear stresses mobilised between successive gauge levels $\tau_{\mathrm{sf}}/q_{\mathrm{c,avg}}$ (where $q_{\mathrm{c,avg}}$ is the average cone resistance between the gauge levels in question) showed a reduction with increasing normalised distance from the base h/D_{b}, the inability to measure local radial stresses during installation, curing and loading ultimately prevented validation of the friction fatigue mechanism for driven cast-in-situ piles.

Base resistance

The ultimate base resistance $q_{\mathrm{b,ult}}$ of a pile in granular soil is typically related to the free-field vertical effective stress at the base $\sigma'_{\mathrm{v0,b}}$ using the following relationship:

$$q_{\mathrm{b,ult}} = N_{\mathrm{q}}\, \sigma'_{\mathrm{v0,b}} \qquad \text{Eqn. 5}$$

where N_{q} is the bearing capacity factor which is typically a function of the soil's angle of friction ϕ' (Berezantsev et al. 1961). Given the difficulties in obtaining undisturbed samples in sands and gravels, the ultimate base resistance of closed-displacement driven piles (at 10% of the pile base diameter) $q_{\mathrm{b,0.1D}}$ is more successfully related to the average cone resistance $q_{\mathrm{c,avg}}$ using the following equation, as recommended by the UWA-05 method (Lehane et al. 2005):

$$q_{\mathrm{b,0.1D}} = 0.6 q_{\mathrm{c,avg}} \qquad \text{Eqn. 6}$$

where $q_{c,avg}$ is the average cone resistance determined using the Dutch q_c averaging method (Schmertmann, 1978). Using a database of 16 No. piles, Flynn and McCabe (2021) showed that Equation 6 provided superior estimates of the base resistance of DCIS piles in granular soils in comparison to other CPT-based methods, with the mean predicted-to-measured resistance ratio of the piles in the database in agreement with those reported for closed-ended driven piles in sand by Xu et al. (2008).

Dynamic testing

Dynamic pile testing is a cost-effective alternative to traditional pile testing methods which require the application of static compression loads to the pile head using either kentledge or a steel test beam connected to ground anchors or tension reaction piles. The dynamic pile testing technique, which was initially developed for precast concrete piles in the 1960s, involves the measurement of wave propagation within a pile induced by the impact of a ram (or hammer in the case of driven piles during installation) at the pile head. By measuring the variation in strain and acceleration at or close to the pile head using diametrically-separated pairs of strain gauges and accelerometers, the variation in mobilised force F and pile velocity v with time after impact can be determined (Figure 2a). In an infinite rod free of resistance, the force is theoretically equivalent to the velocity times pile impedance Z, as defined in Equation 7 (where E is the pile axial elastic stiffness, A is the cross-sectional area of the pile, c is the wave speed of the pile, ρ is the density of the pile material). However, F and Zv will deviate due to end fixity in a finite elastic rod and resistance effects along the rod shaft, consistent with the response of a pile under axial compression load (Hannigan et al. 2016). A comparison of the measured force F and predicted force Zv after impact enables the total pile resistance to be determined using closed-form solutions such as the Case method (Rausche et al. 1972).

$$Z = EA/c = EA/\sqrt{(E/\rho)} \qquad \text{Eqn. 7}$$

Predictions of (i) mobilised total, shaft and base resistances, (ii) the distribution of shear stresses on the shaft of the pile and (iii) the load-displacement response at the pile head and base, for a given blow, may be obtained using the Case Pile Wave Analysis Program or CAPWAP (PDI, 2006). As shown in Figure 2b, this method uses a series of discrete uniform elastic elements to simulate the pile, with the mobilised resistance on the shaft and base of the pile modelled using springs, sliders and dashpots. By solving the mathematical model using one-dimensional wave theory (Smith, 1960), predictions of the time-dependent force response of the pile after impact are obtained. The properties of the springs and dashpots are subsequently adjusted to obtain improved estimates of the measured stress waves in a process referred to as 'signal matching'. The primary variables in this process are the quake q, representing the displacement u required to fully mobilise the static pile resistance Q_{static}, and the damping factor J which accounts for the dynamic component of resistance mobilised after impact due to, for example, rate effects in the soil arising from the pile velocity v (Figure 2b). The total resistance to driving Q_{total} (i.e. the sum of static and dynamic components) can be obtained using the following equation, based on the model by Smith (1960):

$$Q_{\text{total}} = \min\,(u/q,\, 1)\,(1 + Jv)\,\mathrm{Q}_{\text{static}} \qquad \text{Eqn. 8}$$

Equation 8 is applied to the individual elements using quake and damping values appropriate to the pile shaft, as summarised in Table 1, to derive the shaft resistance. The base resistance is derived for the bottom pile element using the same process with appropriate values of quake and damping factors for the base. The dynamic parameters are subsequently adjusted to improve the predicted force trace until a match is obtained with the measured response. However, the signal matching process is often criticised for lacking a unique solution (Fellenius and Massarsch 2008), as various combinations of quake and damping factors may lead to a sufficient match with the measured stress waves, and hence it relies on the experience of the operator. The method also requires sufficient displacement to mobilise the pile resistance beyond the quake, which may occur at a time greater than that at which the waves return to the sensors (referred to as time $2L/c$, where L is distance from the sensors to the pile base). Regardless of these criticisms, the method has been shown to provide reliable estimates of pile resistance, particularly in offshore settings where static load testing is cost-prohibitive (Buckley et al. 2020).

EXPERIMENTAL PROGRAMME

Full-scale DCIS piles were installed at three separate sites in the United Kingdom (Pontarddulais, Dagenham and Ryton-on-Dunsmore; see Figure 3) to compare capacity predictions arising from dynamic load tests during installation with measured static load test capacities following in-situ concreting and curing. The results of the dynamic tests on the DCIS pile tubes were compared to those on (i) precast concrete piles which were installed at Pontarddulais and Dagenham, and (ii) a closed-ended steel pile installed at Pontarddulais.

Ground Conditions

A brief synopsis of the ground conditions encountered at the three sites is provided in this section; further information is available in Flynn (2014), Flynn et al (2012) and Flynn and McCabe (2016, 2019).

Pontarddulais

The site at Pontarddulais is located approximately 12 km northwest of Swansea in Wales. The cone resistance q_c profile at the location of the DCIS test pile is shown in Figure 4a. The ground conditions inferred from the CPTs comprised up to 1.8 m of sand and gravel (historical fill) overlying soft organic clay with peat lenses. At 4.7 mbgl, the cone encountered a layer of medium dense silty sand which in turn was underlain by a layer of firm clay, followed by loose to medium dense silty sand at 7.5 mbgl. Pore pressure measurements during each CPT sounding indicated that the groundwater level was at 2 mbgl.

Dagenham

The Dagenham pile test was carried out on a brownfield site located 1.5 km north of the River Thames and 20 km east of London. Ground investigation information comprised cable percussion boreholes supplemented by CPTs. The stratigraphy at the site comprised made ground of variable composition and anthropogenic material associated with historical industrial activities, overlying very soft to soft marshland deposits of amorphous clay, together with various bands of fibrous peat, followed by an intermixed layer of loose to very dense fine to coarse sands and gravels at a depth of 7.0 mbgl. CPT testing proved difficult within the latter stratum, with numerous refusals occurring at the base of the alluvium; the q_c profiles in the vicinity of the test pile are illustrated in Figure 4b. Perched water tables were routinely encountered within the made ground (due to its variable composition and fines content), with sub-artesian pressures present in sands and gravels due to the relatively impermeable overlying fine-grained soils.

Ryton-on-Dunsmore

The ground conditions at Ryton-on-Dunsmore, south east of Coventry in Warwickshire, comprised a 1.8 m thick layer of clay fill overlying medium dense to dense sand, known colloquially as Baginton Sand. The sand is typically uniformly graded with a mean particle size D_{50} = 0.3 mm and a coefficient of uniformity C_u = 1.69. A series of direct shear box tests on dry air-pluviated samples (Flynn and McCabe 2016) reported a constant volume friction angle ϕ'_{cv} of 35°. The average cone resistance q_c profiles of three CPTs in the vicinity of the test piles is shown in Figure 4c. An in-situ small strain shear stiffness G_0 of approximately 110 MPa was inferred for the sand layer using a seismic cone penetrometer performed in the centre of the test area. No pore pressures were observed during penetration in each test and groundwater monitoring at an adjacent site indicated that the groundwater level was in excess of 15 mbgl.

Test Pile Details

Relevant details of the instrumented DCIS piles (Pontarddulais (P1), Dagenham (D1) and Ryton-on-Dunsmore (R1, R2 and R3)) are provided in Table 2. All DCIS piles were constructed using a 320mm outer diameter 20mm thick steel tube fitted with a 380mm diameter and 10mm thick base plate. In order to measure the shaft and base resistances during static loading, the reinforcement cage for each DCIS test pile was instrumented with sister-bar vibrating wire strain gauges at four separate levels (one of which was near the pile base), with four gauges at each level to capture bending effects. The gauge level positions were chosen to optimize the measurement of shaft resistance across soil layers (particularly important at the layered soil sites at Dagenham and Pontarddulais).

In addition, details of tests on other displacement pile types subject to dynamic loading at Pontarddulais (two 250mm square precast concrete piles: PCC1 and PCC2, and a single 140mm diameter steel closed-ended pile: CEP1) and Dagenham (a 275mm square precast concrete pile: PCC3) are also presented in Table 2.

Installation and dynamic load testing

The DCIS pile tubes were installed using either four or five tonne Junttan HHK hydraulic hammers. Due to the oversized driving shoe, a gap developed between the exterior of the tube and the soil at the ground surface during driving of all test piles (Figure 5a). Each DCIS test pile installation was monitored dynamically during driving using a diametrically-separated pair of accelerometers and strain gauges mounted to the outer wall of the steel installation tube prior to driving (Figure 2a). The instrumentation was connected to a Pile Driving Analyzer (PDA) in order to measure the induced stress waves, dynamic resistance and energy transferred to the tube during driving. CAPWAP signal matching was undertaken by suitably-qualified operators from commercial testing companies on blows selected by the authors during the initial and intermediate stages of driving, as well at the end-of-driving (subsequently denoted EOD). The primary purpose of the CAPWAP analyses was to assess the mobilised shaft and base resistances on the installation tube and base plate, respectively, during driving. The maximum displacement of the installation tube during each dynamic test, typically denoted DMX (Hannigan et al. 2016), ranged from 19 to 26mm, but was locally up to 65mm for Pile P1.

Upon completion of driving to the required depth, the steel installation tube was filled with high slump concrete and subsequently retracted. To ensure the concrete was adequately compacted and free of any voids, the tube was subjected to several hammer blows during the withdrawal process. Following completion of the pile, the reinforcement cage was inserted into the freshly cast concrete, as shown in Figure 5b.

Piles PCC1, PCC2 and CEP1 at Pontarddulais were also subject to dynamic testing during installation. While PCC3 at Dagenham was not subjected to a dynamic test during driving, a dynamic restrike test was performed approximately 10 days after installation. CAPWAP signal matching was also conducted for these piles.

Curing

The DCIS test piles were left to cure for a period of 9 to 24 days to enable the concrete to gain sufficient strength prior to static load testing. The strains and temperatures within test pile D1 at Dagenham were monitored at regular intervals (every 15 mins, increased to hourly after 25 hours) during curing in order to assess the development of residual loads; these include internal processes such as the restraint arising from shrinkage and swelling and external processes such as dragloads associated with consolidation of the alluvium resulting from upfilling and dissipation of excess pore pressures during driving of the steel installation tube in this case. Further details of the strain and temperature measurements during curing of pile D1 are presented by Flynn et al. (2012).

Static load testing

The test piles were subjected to maintained compression load tests using a steel testing frame anchored to DCIS reaction piles (Figure 5c). The reaction piles were constructed at a minimum distance equivalent to eight pile diameters from the test pile (ICE, 2007) in order to minimise interaction effects. The test instrumentation comprised a load cell, hydraulic jack, displacement transducers and a data acquisition unit. The load applied during the tests was measured using a 3000 kN capacity load cell, calibrated prior to use, which was placed between the underside of the loading frame and the hydraulic jack. Four linear potentiometric displacement transducers (LPDT), rigidly mounted to an independent aluminium reference beam, were used to measure the pile head displacements upon flat surfaces attached to the side of the pile cap. Data during loading were acquired using a Campbell Scientific datalogger which was connected to the LPDTs, load cell and strain gauge instrumentation. A digital thermometer was also used to monitor the ambient temperature throughout the duration of the load test.

The maintained compression load tests on the instrumented DCIS piles P1 and D1 were performed in accordance with the Institution of Civil Engineers Specification for Piling and Embedded Retaining Walls *or* SPERW (ICE, 2007) which is the standard specification for static load testing of piles in the United Kingdom. Loading was performed in several stages, with the increment size based on the design verification load (DVL) of the pile which was calculated by dividing the estimated total capacity (determined by either earth pressure or CPT-based methods) by the geotechnical factor of safety. Cycling (i.e. a single unload-reload loop) was also performed at applied loads corresponding to 100 % DVL and 100 % DVL + 50% SWL, where SWL is the specified working load. The test piles at Ryton-on-Dunsmore (R1, R2 and R3) were not performed in accordance with ICE SPERW as, unlike at the other sites, these tests were not part of a commercial piling contract and hence were loaded in increments equivalent to 10% of the predicted compression capacity, reducing to 5% when pile failure was imminent, without unload-reload loops.

Derivation of the load distribution from the measured strains in each pile during static loading was determined using the secant modulus method (Lam and Jefferis, 2011). As the test piles were not exhumed after testing, the shaft diameters of the piles were assumed to correspond to the driving plate diameters at the base of the installation tube in order to provide conservative lower-bound estimates of the mobilised shear stresses (Flynn and McCabe 2021). Further details of the interpretation process are presented in Flynn (2014).

RESULTS

Installation

Driving records

The driving records (number of blows per 250mm penetration) for the DCIS piles at Pontarddulais (P1), Dagenham (D1) and Ryton-on-Dunsmore (R1, R2 and R3), are presented in Figures 6(a), 6(b) and 6(c) respectively. At Pontarddulais and Dagenham, the blow counts varied considerably during driving (primarily due to the layered stratigraphy at both sites), with the installation tube tending to plunge through the soft alluvial layers under a single hammer blow. A strong increase in resistance was noted at Dagenham once the installation tube penetrated the underlying dense sands and gravels, with driving terminated at 7.7 mbgl when the blowcount had reached 20 blows/250mm. The measured blow counts per 250mm at Pontarddulais were considerably lower due to the loose nature of the sands and gravels at the site in comparison to Dagenham, with 4 blows/250mm recorded upon reaching the required toe level. The corresponding final blowcounts for the Ryton-on-Dunsmore piles were in the range 15-24 blows/250mm.

Figure 6a also illustrates the installation records for the 250mm square precast concrete piles PPC1 and PPC2, as well as the 140mm diameter closed-ended steel pile CEP1, which were also driven at the Pontarddulais site using a similar hammer and drop height to P1. Despite having smaller shaft and base areas in comparison to DCIS Pile P1, the number of blows required for 250mm penetration for PPC1, PPC2 and CEP1 were all double or greater than that recorded for Pile P1 after penetration below the soft layers (i.e. beyond a depth of 6.0m). Given that the installation tube of the DCIS pile is analogous to a traditional closed-ended circular pile, the reduced resistance to driving may be attributed to the oversized driving shoe at the base of the tube and its effect on the mobilised resistance on the external shaft of the installation tube. This effect is explored in more detail in conjunction with the dynamic test results during installation in the following section.

Dynamic measurements

Figures 7 shows the variation in measured force F and velocity times impedance Zv traces with time after impact (as multiples of L/c) at the end-of-driving of the installation tube for the DCIS test piles P1 and D1, while the corresponding dynamic traces for R1 to R3 are illustrated in Figure 8. The traces for selected blows at the intermediate depths (identified in Table 2) during driving of the DCIS test piles are presented as Figures S1 to S7 in Supplementary Information. The initial values of F and Zv shown on the figures represent hammer impact (at negative values of time), with peak values occurring at a time of zero where the wave first passes the sensor. The following points are noteworthy:

- The F and Zv traces for each pile show minimal separation for the majority of the period between impact and return of the waves to the sensors at time $2L/c$.
- Approaching time $2L/c$, F and Zv begin to diverge rapidly, with F becoming negative (i.e. tensile) and Zv increasing as the pile accelerates downwards.
- The above pattern typically repeated for the remainder of each trace after time $2L/c$ as the waves travel up and down the tube; this repetitive pattern was most apparent for pile P1.

The minimal separation in the stress waves until time $2L/c$, and repetitive cyclic nature thereafter, implies that little resistance was mobilised on the shaft of the installation tube during driving, with the rapid increase in Zv approaching time $2L/c$ indicative of a tension wave in the installation tube induced by an apparent free-end condition at the base, as the tube tended to plunge or '*run*'. Given that no physical connection exists between the installation tube and sacrificial base plate to resist tension, this observation would suggest that a gap may open at this location due to tensile force in the tube.

The measured dynamic responses of the precast concrete pile PPC1 and closed-ended steel pile CEP1 at the end-of-driving at Pondarddulais are shown in Figure 9a and 9b, respectively, while Figure 9c illustrates the response of precast pile PCC3 during a restrike test at Dagenham. In contrast to the measurements for the DCIS piles during installation, the Zv traces exhibited a large divergence from the F waves between 0 and $2L/c$, which is indicative of greater resistance encountered along the pile shaft for these piles. Furthermore, the responses of the three traditional displacement piles after $2L/c$ were notably different when compared to the DCIS piles, with the Zv trace becoming tensile and the F trace remaining relatively constant or slightly increasing during the period up to about $8L/c$. These stark differences prompted a quantitative CAPWAP analysis of load-settlement behaviour of the DCIS piles, interpreted in the next section in conjunction with the static load tests.

Load settlement behaviour – CAPWAP analyses and static load tests

CAPWAP analyses during installation

The total, shaft and base load-displacement responses of the installation tube predicted by CAPWAP signal matching of stress waves at the end-of-driving for each site are illustrated in Figure 10 for Pontarddulais and Dagenham, and Figure 11 for Ryton-on-Dunsmore. As expected from inspection of the dynamic wave traces obtained by the PDA instrumentation, the majority of total resistance was generated on the underside of the driving shoe at the base of the installation tube.

Static load tests

Figures 10 and 11 also illustrate the mobilisation of total, shaft and base resistance with pile displacement of the DCIS piles during static compression loading which were obtained from the strain gauge instrumentation installed in each pile after in-situ concreting. In contrast with the observations during driving, it is evident that the shaft resistance accounts for a substantial portion of the total pile resistance during static loading, ranging from 30% for D1 to 83% for P1; this implies that some level of recovery in radial stresses (and hence shear stresses during loading) occurred following in-situ concreting of the pile after driving. However, the estimates of base resistance of the installation tubes from the CAPWAP analyses are more comparable with those measured under static loading, particularly at Ryton-on-Dunsmore. The under-predictions of base resistance at Dagenham and Pontarddulais may be partly explained by the residual base loads mobilised on the test piles prior to static loading arising from dragloads induced by on-going settlement in the overlying soft clay layers (Flynn et al. 2012, Flynn 2014), as well as the lower pile displacement mobilised during the dynamic load test at the end-of-driving (as evident for the test pile at Dagenham). Improved predictions of base resistance are obtained when these dragloads are included for these piles (Figure 10), particularly for Pile P1.

Figure 12 presents the respective distributions of unit shear stress at failure with depth inferred between successive gauge levels for piles P1 and D1, while Figure 13 shows the corresponding distributions for R1, R2 and R3. Also included in Figures 12 and 13 are the predicted unit shear stress distributions from the CAPWAP analyses from the dynamic load tests at the end-of-driving of each test pile. Whilst it is acknowledged that the inferred values of shear stress from the CAPWAP analyses are a function of the displacement induced, as well as the quality of the signal match obtained by the operator, it is clearly evident from these figures that the mobilised shear stresses during static compression load are significantly greater than those on the external shaft of the installation tube during driving. Furthermore, the magnitude of the shear stresses on the installation tube inferred from the CAPWAP analyses are below 50 kPa (and below 20 kPa in most cases) over the majority of the embedded tube length, regardless of the ground conditions. As such, the resistance to driving for the test piles at each site was almost exclusively due to end-bearing resistance on the underside of the sacrificial base plate.

The variations in shear stresses on the installation tube and as-constructed DCIS piles during dynamic and static load testing at Pontarddulais and Dagenham were also compared with those from the dynamic tests performed on precast concrete piles at both sites. As shown in Figure 12(a), the inferred distribution of shear stresses along the embedded length of the precast pile from the CAPWAP signal-matching analyses exceed those on the installation tube of the DCIS pile (below a depth 4m) during driving. A similar conclusion can be drawn from the restrike test on PCC3 at Dagenham approximately 10 days after installation (Figure 12b). However, the mobilised shear stresses on the DCIS test piles during static loading were significantly greater than those for the precast piles at both sites, with such increases arising from the enhanced roughness of the DCIS piles created by in-situ concreting in granular strata with coarse angular particles, particularly the Thames Gravels present at Dagenham. These particles, in conjunction with the rougher shaft interface, promote enhanced shearing and dilation under loading which cannot be matched by the smoother interface of a precast concrete pile.

It is important to note that differences in geometry (square, circular), material type (steel, concrete), surface roughness (steel, precast concrete, cast-in-situ concrete) and time-related effects (ageing / soil set-up due to consolidation) may influence the comparison of shear stresses for the steel installation tubes, as-built DCIS piles and precast concrete or steel piles. Nonetheless, the increases in shear stresses observed at the time of static load testing of the DCIS test piles (which were two to five times greater than those inferred from CAPWAP analyses on the installation tube) cannot be solely attributed due to the differences noted above and hence are explored in more detail in the next section.

DISCUSSION

The negative effect of oversized driving shoes on the shaft resistance of displacement piles has been reported in the literature. For example, Finlay et al. (2001) investigated the effects of internal and external shoes on the shaft resistance of 319mm outer diameter, 17mm thick, open-ended steel piles installed in sand. The piles were instrumented with radial stress sensors to capture the variations in internal and external radial stresses during jacking, with the results showing a four-fold reduction in external radial stresses (and hence shear stresses) when the piles were fitted with a driving shoe with a diameter that was 9% larger than the external shaft diameter. Crucially, the reductions in radial stress were sufficient to bring the soil into a state of active failure after flowing around the oversized driving shoes.

For DCIS pile installation tubes having 508mm outer diameter, Verstraelen et al. (2016) reported a reduction of up to 15% in the shaft resistance upon replacing the standard 550mm diameter base plate (8% oversized) with a 600mm diameter base plate (18% oversized). In practice, however, the base plate oversize percentage for DCIS piles is typically greater than the standard 8% value used by Verstraelen et al. (2016), and indeed the 9% value modelled by Finlay et al. (2001). The diameters of driving shoes used at the three test sites in this paper were oversized by approximately 19%, in keeping with the average value of 15% from the DCIS pile database (excluding Franki piles) compiled by Flynn and McCabe (2021). Hence, the evidence is convincing that the abnormally low shear stresses mobilised on the external shaft of the DCIS installation tube are due to active failure of the soil after flowing past the oversized driving shoe.

Following in-situ concreting and curing, the mobilised shear stresses on the shaft of the DCIS piles during static compression load testing at the three sites were typically two to five times greater than those on the exterior of the steel installation tube inferred from dynamic testing during driving. The average radial effective stress acting between successive gauge levels on the shaft of each DCIS test pile during static loading may be tentatively inferred from the corresponding shear stress at $\tau_{sf,}$ using

Equation 2 with $\delta = \phi'_{cv} = 35^\circ$ from shear box tests at Ryton-on-Dunsmore and for the remaining sites, 33° for siliceous sand (Bolton, 1986) and 38° for gravel (Paul et al., 1994). The total radial stress is then obtained by $\sigma_{r,i} = \sigma'_{r,i} + u_i$, where u_i is the hydrostatic pore pressure at the mid-point between the gauge levels in question. Figure 14 presents the distribution of $\sigma_{r,i}$ with depth for the piles at the three test sites, as well as additional pile data for sites at Erith and Shotton reported by Flynn (2014). Also shown in Figure 14 is the theoretical bi-linear distribution of radial total stress with depth induced by the fluid pressure of freshly-cast concrete $\sigma_{r,conc}$ using Equation 9 proposed by Lings et al. (1994):

$$\sigma_{r,conc} = \gamma_c z \qquad \text{for } z \leq h_{crit} \qquad \text{Eqn. 9a}$$

$$\sigma_{r,conc} = \gamma_w z + (\gamma_c - \gamma_w)\, h_{crit} \qquad \text{for } z > h_{crit} \qquad \text{Eqn. 9b}$$

where γ_c is the unit weight of fluid concrete (taken as 24 kN/m^3), γ_w is the unit weight of water, z is the depth below top of concrete fluid and h_{crit} is the critical depth. Lings et al. (1994) define h_{crit} as the depth equivalent to one-third of the head of concrete cast which, for the dataset in Figure 14 with pile lengths ranging from 5.5 to 11.0m, results in h_{crit} varying from 1.8 to 3.7 mbgl. It is evident that the theoretical radial total stress induced by the wet concrete forms a lower-bound to the radial stresses inferred from the shear stresses on the shaft of the test piles, indicating that the reductions in radial stress during installation due to the over-sized base plate are recoverable by the concreting process. Further increases in radial stress, over and above those predicted by Equation 9, are likely to be attributed to enhanced interface dilation on the rough surface of the pile shaft created by in-situ concreting.

An unanticipated finding from the Flynn and McCabe (2021) DCIS pile database was that the simplified LCPC-82 method (Bustamante and Gianeselli 1982) produced better predictions of DCIS pile shaft resistance than the more advanced UWA-05 (Lehane et al. 2005) and ICP-05 (Jardine et al. 2005) methods. In Figure 14, the radial total stresses appear to be distributed somewhere between the bi-linear distribution of fluid pressure with depth and constant (no variation) with depth. Therefore, the relative success of the LCPC-2A in predicting the variation in DCIS pile shaft resistance with embedment length may be related to its weaker stress level dependence, compared to the UWA-05 and ICP-05 methods which use non-linear functions to model the reduction in shear stresses with normalised distance h/D_b from the pile base. Unfortunately, as previously mentioned, definitive conclusions in relation to changes in shear stresses following installation, casting, curing and load testing cannot be reached in the absence of radial stress measurements at present.

Figure 15 shows a comparison of the base resistances inferred from CAPWAP analyses of selected blows during driving of the installation tubes with the measured base resistance from the five static load tests at the three sites. In contrast to the discrepancies in shaft resistance observed between installation and static loading, the base resistance of the DCIS piles remained relatively unchanged. This is expected however, as the steel driving shoe remains at the base of the pile following casting of the concrete and withdrawal of the installation tube and hence would not be affected by loosening or stress relief to the same extent as the pile shaft. Hence, the base resistance of a DCIS pile may be inferred reliably from the results of a dynamic load test on the steel tube during installation. Also shown in Figure 15 are the profiles of base resistance $Q_{b,0.1Db}$ predicted from the measured cone resistance q_c profiles at each pile location using Equation 6. Whilst some degree of scatter in the CAPWAP results is evident (given the aforementioned issues with interpretation of the dynamic tests, in particular the partial mobilisation of resistance due to insufficient displacement induced during the test), the inferred base resistances from the CAPWAP analyses are comparable with Equation 6 over a wide range of embedded lengths (with the exception of Pontarddulais, where the residual load represented a significant portion of the base resistance prior to static load testing), indicating that the results of dynamic load tests on the steel tube during installation can provide reasonable first-order estimates of the base resistance for DCIS piles. The static load test on Pile R3 resulted in a considerably larger base resistance than predicted by the dynamic test during installation; however, as discussed by Flynn and McCabe (2016), this pile exhibited an unexpectedly higher total resistance than envisaged (with the test terminated at the maximum allowable load of the reaction frame). Given that the dynamic test predicted a base resistance which is in agreement with that estimated by Equation 6, it is postulated that the additional resistance of the pile during the load test was generated by the underside of the pile cap bearing on the ground; ignoring this additional resistance results in an over-estimation of the base resistance in the static load test, as illustrated in Figure 15.

In summary, the dynamic tests showed that low shaft resistances were mobilised on the steel tube during installation which were attributed to loosening of soil after flowing around the oversized driving shoe at the base of the installation tube, inducing active conditions. However, the maintained compression load tests on the instrumented DCIS test piles demonstrated that any reductions in shaft resistance resulting from the use of the oversized driving shoe were subsequently recoverable. This outcome contrasts with design practice in Belgium (NBN, 2014; Huybrechts et al. 2016) which stipulates that the shaft resistance of DCIS piles must be ignored when an oversized driving shoe (with a diameter at least 50mm greater than the installation tube) is utilised during installation and would result in excessive design lengths if applied to the test piles in this study.

CONCLUSIONS

A series of dynamic load tests were performed on the temporary steel driving tubes during the installation of DCIS piles at three sites in the United Kingdom. The piles were subsequently instrumented with strain gauges after concreting and subjected to maintained compression load tests to failure after a suitable curing period. The shear stresses mobilised on the shaft of the as-constructed DCIS piles during the maintained load testing were two to five times greater than those inferred from the results of the dynamic tests on the steel installation tube during driving. This was primarily attributed to the loosening of soil on the shaft of the installation tube arising from the over-sized sacrificial driving shoe at the base. However, the reductions in radial stress are likely to be reversible by the fluid pressures from the freshly-cast concrete which were shown to provide lower-bound estimates of radial total stresses tentatively inferred from the measured shear stresses during static loading. The recovery of shaft resistances following concreting and curing conflicts with European design practice (which neglects the shaft resistance of a DCIS pile when an oversized driving shoe is utilised), resulting in overly-conservative design lengths if applied to the test piles in this study. Whilst the shaft resistance of DCIS piles was significantly underpredicted by the dynamic load tests during installation, reasonable estimates of the base resistance were obtained.

Based on the foregoing, the practice of relying solely on dynamic tests performed on the installation tube to predict the total capacity of DCIS piles is inappropriate. However, this should not be interpreted as an outright rejection of dynamic testing for DCIS piles; there is merit in performing such tests on the final concrete pile, once it has gained sufficient compressive strength and the shaft resistance has developed.

Acknowledgements

The authors wish to acknowledge Keller Foundations for sponsoring a comprehensive programme of DCIS pile testing, of which this driveability study formed part. The views expressed in this paper are solely the opinions of the authors and do not represent the views of Keller Foundations. The first author was sponsored by the College of Engineering and Informatics Fellowship and University Foundation Bursary during his doctoral studies at NUI Galway.

REFERENCES

Berezantsev, V.G., Khristoforov, V.S. and Golubkov, V.N. 1961. Load bearing capacity and deformation of piled foundations. In: Proceedings of the 5th International Conference on Soil Mechanics and Foundation Engineering. Paris, France. 11–15.

Bustamante, M. & Gianeselli, L. (1982). Pile bearing capacity prediction by means of static penetrometer CPT. *Proc. 2^{nd} European Symp. on Penetration Testing*, Amsterdam, The Netherlands. pp. 493-500.

Bolton, M.D. 1986. The strength and dilatancy of sands. Géotechnique, Vol. 36(1): 65-78.

BSI. 2015. Code of Practice for Foundations. BS8002:2015. British Standards Institute (BSI), London, United Kingdom.

Buckley, R.M., Kontoe, S., Jardine, R.J., Barbosa, P. and Schroeder, F.C. 2020. Pile driveability in low-to-medium density chalk. Canadian Geotechnical Journal, DOI: 10.1139/cgj-2019-0703, In Press.

CEN. 2004. Eurocode 7: Geotechnical Design – Part 1: General Rules. EN 1997-1-2004. Comité Européen de Normalisation (CEN), Brussels, Belgium.

DGG. 2013. Recommendations on Piling (EA-Pfahle*)*. Deutsche Gesellschaft fur Geotechnik (DDG) e.V, Wiley Ernst & Son.

Fellenius, B.H. 2020. Basics of Foundation Design. Retrieved from www.fellenius.net/papers.html. July 2020.

Fellenius, B.H. and Massarsch, K.R. 2008. Comments on the current and future use of pile dynamic testing. In: Proceedings of the 8^{th} International Conference on the Application of Stress-Wave Theory to Piles, Lisbon, Portugal, pp. 7–17.

Finlay, T.C.R., White, D.J., Bolton, M.D. & Nagayama, T. 2001. Press-in piling: the installation of instrumented steel tubular piles with and without driving shoes. In: Proceedings of the 5th International Conference on Deep Foundation Practice, Singapore, pp. 199-208.

Fleming, W.G.K., Weltman, A., Elson, K. & Randolph, M.F. 2008. Piling Engineering. Taylor & Francis, London.

Flynn, K.N. 2014, Experimental investigations of driven cast-in-situ piles. PhD Thesis. National University of Ireland, Galway, Ireland.

Flynn, K.N., McCabe, B.A. 2016. Shaft resistance of driven cast-in-situ piles in sand. Canadian Geotechnical Journal, Vol. 53 (1), 49-59.

Flynn, K.N and McCabe, B.A. 2019. Driven cast-in-situ piles installed using hydraulic hammers: installation energy transfer and driveability assessment. Soils and Foundations, Vol. 59(6), 1946–1959.

Flynn, K.N and McCabe, B.A. 2021. Applicability of CPT capacity prediction methods to driven cast-in-situ piles in granular soil. Journal of Geotechnical and Geoenvironmental Engineering, Vol. 147, No. 2, 04020170.

Flynn, K.N., McCabe, B.A. and Egan, D. 2012. Residual load development in cast-in-situ piles – a review and new case history. In: Proceedings of the 9th International Conference on Testing and Design Methods for Deep Foundations (IS Kanazawa), 18-20th September 2012, Kanazawa, Japan, pp. 765–773.

Hannigan, P.J., Rausche, F., Likins, G.E., Robinson, B.R. and Becker, M.L. 2016. Geotechnical Engineering Circular No. 12 – Volume II Design and Construction of Driven Pile Foundations. U.S. Federal Highway Administration, Washington D.C., USA, Publication No. FHWANHI-16-010.

Huybrechts, N., De Vos, M., Bottiau, M. and Maertens, L. 2016. Design of piles – Belgian practice. In: Proceedings of the International Symposium on Design of Piles in Europe (ETC3), Leuven, Belgium, Vol. 2, pp. 7-44.

Institution of Civil Engineers. 2007. Specification for Piling and Embedded Retaining Walls. Thomas Telford, United Kingdom.

Jardine, R.J, Chow, F.C., Overy, R.F. & Standing, J.R. 2005. ICP design methods for driven piles in sands and clays. Thomas Telford, London, UK.

Lam, C. and Jefferis, S.A. 2011. Critical assessment of pile modulus determination methods. Canadian Geotechnical Journal, Vol. 48(10), 1433–1448.

Lehane, B.M., Jardine, R.J., Bond, A.J. and Frank, R. 1993. Mechanisms of Shaft Friction in Sand from Instrumented Pile Tests. Journal of Geotechnical Engineering, Vol. 119(3), 19–35.

Lehane, B.M., Schneider, J.A. and Xu, X. 2005. The UWA-05 method for predction of axial capacity of driven piles in sand. *In* Proceedings of the 1st International Conference on Frontiers in Offshore Geotechnics, Perth, Australia, pp. 683–689.

Likins, G. E. and Rausche, F. 2004. Correlation of CAPWAP with Static Load Tests. In: Proceedings of the 7th International Conference on the Application of Stresswave Theory to Piles, Malaysia, pp. 153-165.

Lings, M.L., Ng, C.W.W. and Nash. D.F.T. 1994. The lateral pressure of wet concrete in diaphragm panels cast under bentonite. Proceedings of the ICE: Geotechnical Engineering, Vol. 107(2), 163 – 172.

NBN. 2014. Eurocode 7: Calcul géotechnique – Partie 1: Refles generals – Annexe nationale. NBN EN 1997-1 ANB, Bureau de Normalisation, Brussels, Belgium.

NEN (2019). Nationale bijlage bij NEN-EN 1997-1 Eurocode 7: Geotechnisch ontwerp – Deel 1: Algemene regels. Koninklijk Nederlands Normalisatue-instituut, July 2019

Paul, T.S., Lehane, B.M., Chapman, T.J.P. & Newman, R.L. 1994. On the properties of a sandy gravel. Proc. 13th Int. Conf. on Soil Mechanics and Foundation Engineering, New Delhi, India. pp. 29-32.

PDI. 2006. CAPWAP Case Pile Wave Analysis Program Version 2006 Background Report. Pile Dynamics Incorporated (PDI), Cleveland, Ohio, USA.

Rausche, F., Moses, F. and Goble, G. 1972. Soil resistance predictions from pile dynamics. Journal of the Soil Mechanics and Foundations Division, Vol. 98 (9), 917-937.

Schmertmann, J.H. 1978. Guidelines for cone penetration test, performance and design. U.S. Federal Highway Administration. Publication No. FHWA-TS-78-209, Washington D.C., USA.

Smith, E.A.L. 1960. Pile-driving analysis by the wave equation. Journal of the Soil Mechanics and Foundations Division, Proceedings of the American Society of Civil Engineering, SM4, 35 – 61.

Verstraelen, J., Maekelberg, W. & Medaets, M. 2016. Recent experiences with static pile load testing on real job sites. Design of Piles in Europe – How did Eurocode 7 change daily practice?, Leuven, Belgium, Volume 1, pp 63-85.

Xu, X., Schneider, J.A. & Lehane, B.M. 2008. Cone penetration test (CPT) methods for end-bearing assessment of open- and closed-ended driven piles in siliceous sand. Canadian Geotechnical Journal, Vol. 45(8), 1130-1141.

LIST OF TABLES

Table 1. Typical dynamic soil parameters for CAPWAP analyses

Dynamic Soil Parameter	Quake q (mm)	Damping factor J (s/m)
Shaft	2.5	0.16 to 0.65
Base	$D_b/60$ to $D_b/120$, where D_b = pile base diameter	0.15

Table 2: Summary of pile and testing details

Site	Pile Type	Pile Ref	Shaft / tube diameter / width (mm)	Base / driving shoe diameter / width (mm)	Length (m)	Dynamic test during driving	Dynamic test during restrike	Static load test after curing/ equalisation	Depth(s) of dynamic load test (m)	Depth of static load test (m)	Curing/ Equalisation period between installation and static load test or restrike (days)
Pontarddulais	DCIS	P1	320	380	8.5	✓		✓	1.2, 8.5	8.5	9
	PC	PCC1	250	250	10.5	✓			10.5	-	-
	PC	PCC2	250	250	10.5	✓			10.5	-	-
Dagenham	CES	CEP1	140	140	9.8	✓			9.8	-	-
	DCIS	D1	320	380	7.7	✓		✓	1.6, 7.4, 7.7	7.7	14
	PC	PCC3	275	275	7.8		✓		7.8	-	10
Ryton-on-Dunsmore	DCIS	R1	320	380	6.0	✓		✓	6.0	6.0	20
	DCIS	R2	320	380	7.0	✓		✓	3.5, 5.3, 7.0	7.0	21
	DCIS	R3	320	380	5.5	✓		✓	3.5, 4.5, 5.5	5.5	24

DCIS = driven cast-in-situ, PC = precast, CES = closed-ended steel

LIST OF FIGURES

Fig. 13. Variation in mobilised unit shear stress with depth at Ryton-on-Dunsmore for (a) Pile R1, (b) Pile R2 and (c) Pile R3.

Fig. 14. Comparison of inferred radial total stress and fluid concrete pressure with depth for DCIS piles.

Fig. 15. Comparison of mobilised base resistance for dynamic and static load tests with predicted base resistance using Equation 6 at (a) Pontarddulais, (b) Dagenham and (c) Ryton-on-Dunsmore.

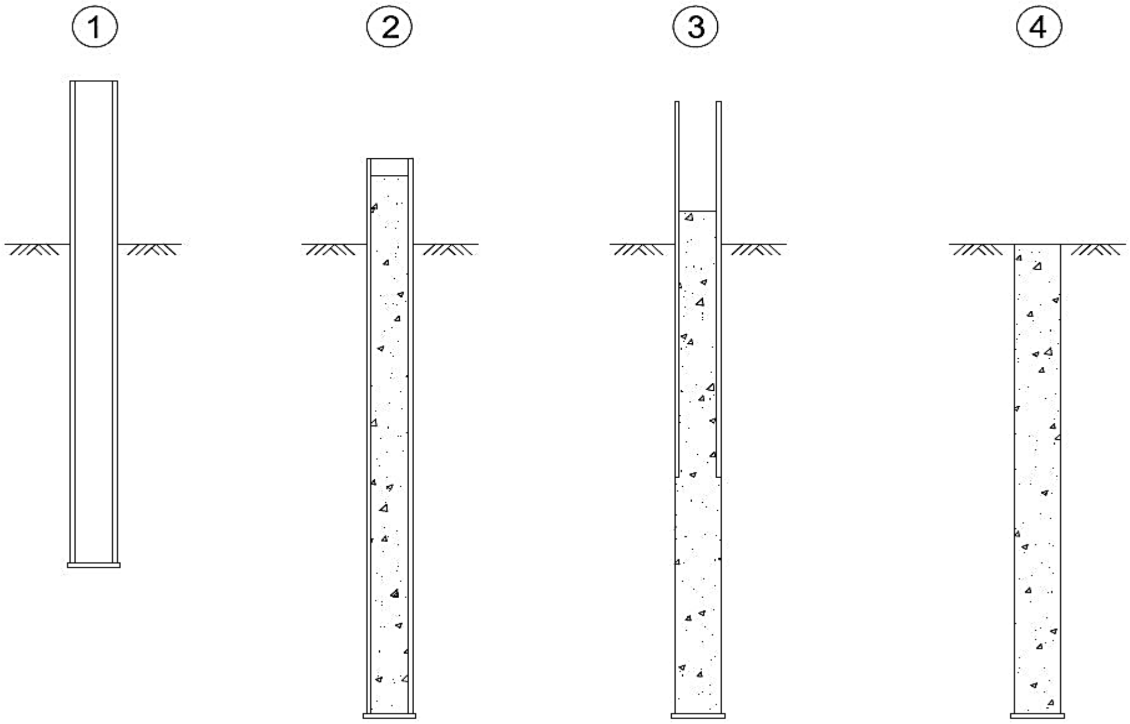

1. Steel tube with sacrificial shoe at the base driven to required depth/set.
2. Tube filled with high-slump concrete.
3. Tube extracted, shoe remains at the base of the pile.
4. Pile left to cure in-situ prior to testing and/or application of structural loads. Reinforcement may be inserted prior to casting or after extraction of tube.

Fig. 1. Schematic of driven cast-in-situ pile construction (adapted from Flynn and McCabe 2016)

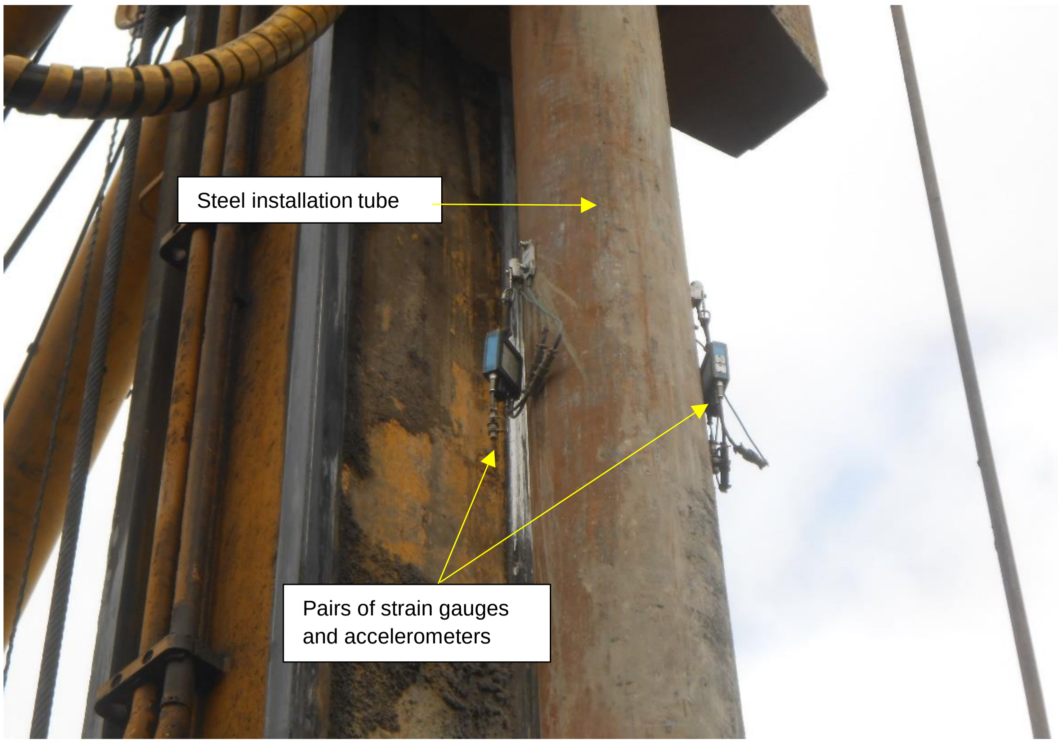

(a)

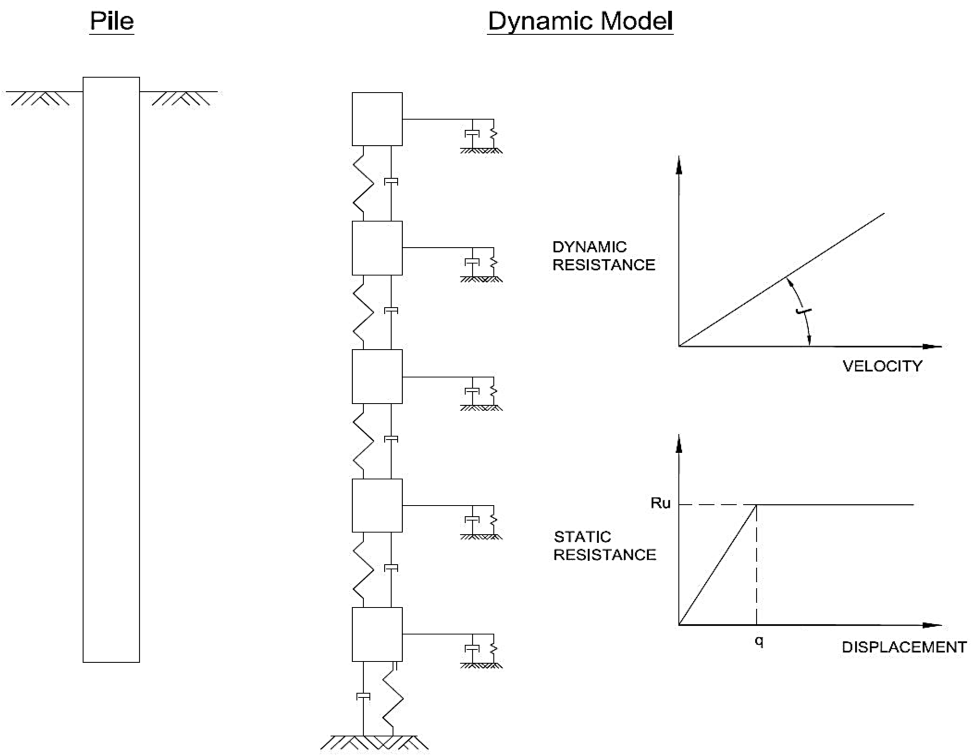

(b)

Fig. 2. (a) Dynamic load test instrumentation and (b) pile and dynamic soil resistance model for CAPWAP analyses.

Fig. 3. Test site locations

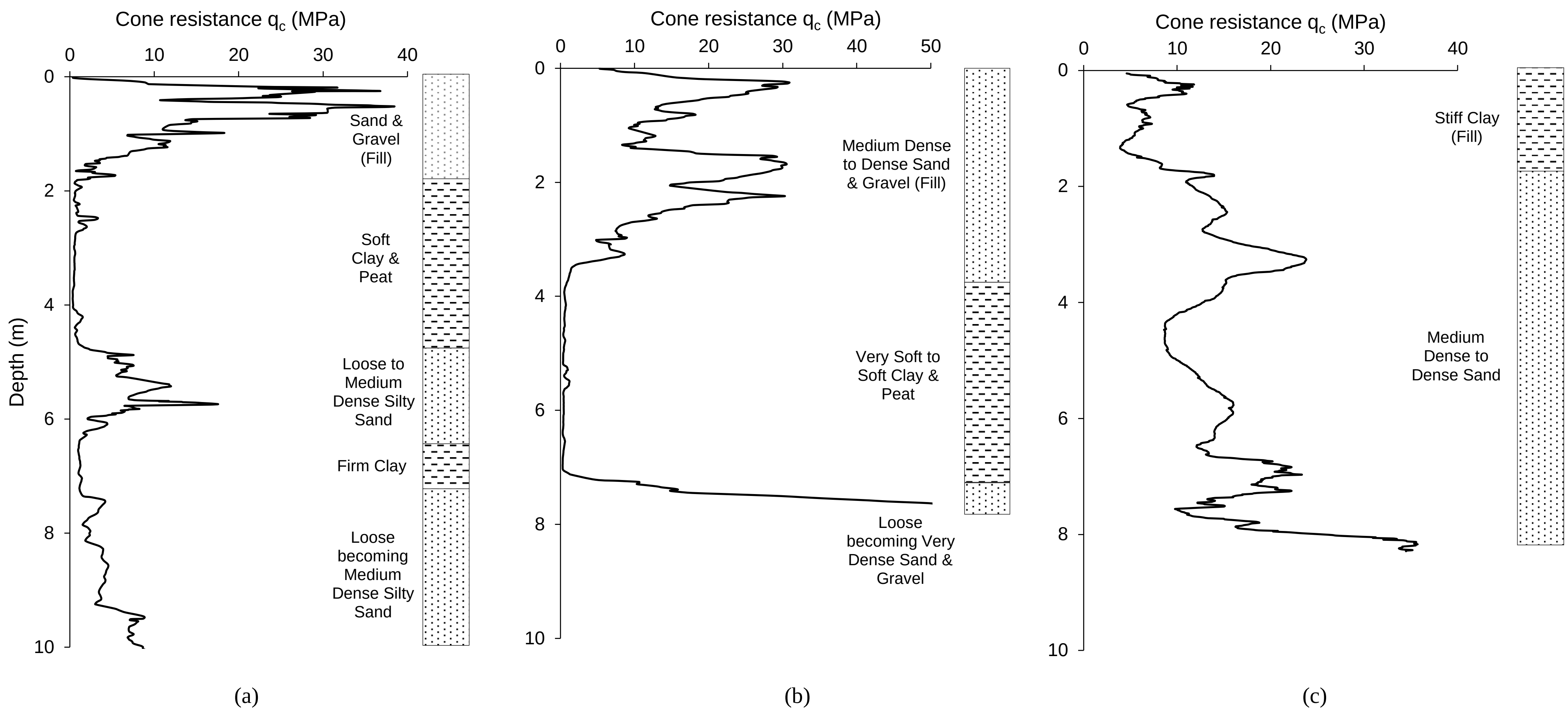

Fig. 4. Cone resistance and ground profiles at (a) Pontarddulais, (b) Dagenham and (c) Ryton-on-Dunsmore

(a) (b) (c)

Fig. 5. (a) Formation of soil gap during driving at Ryton-on-Dunsmore, (b) instrumented reinforcement cage installation at Pontarddulais and (b) static load testing at Ryton-on-Dunsmore.

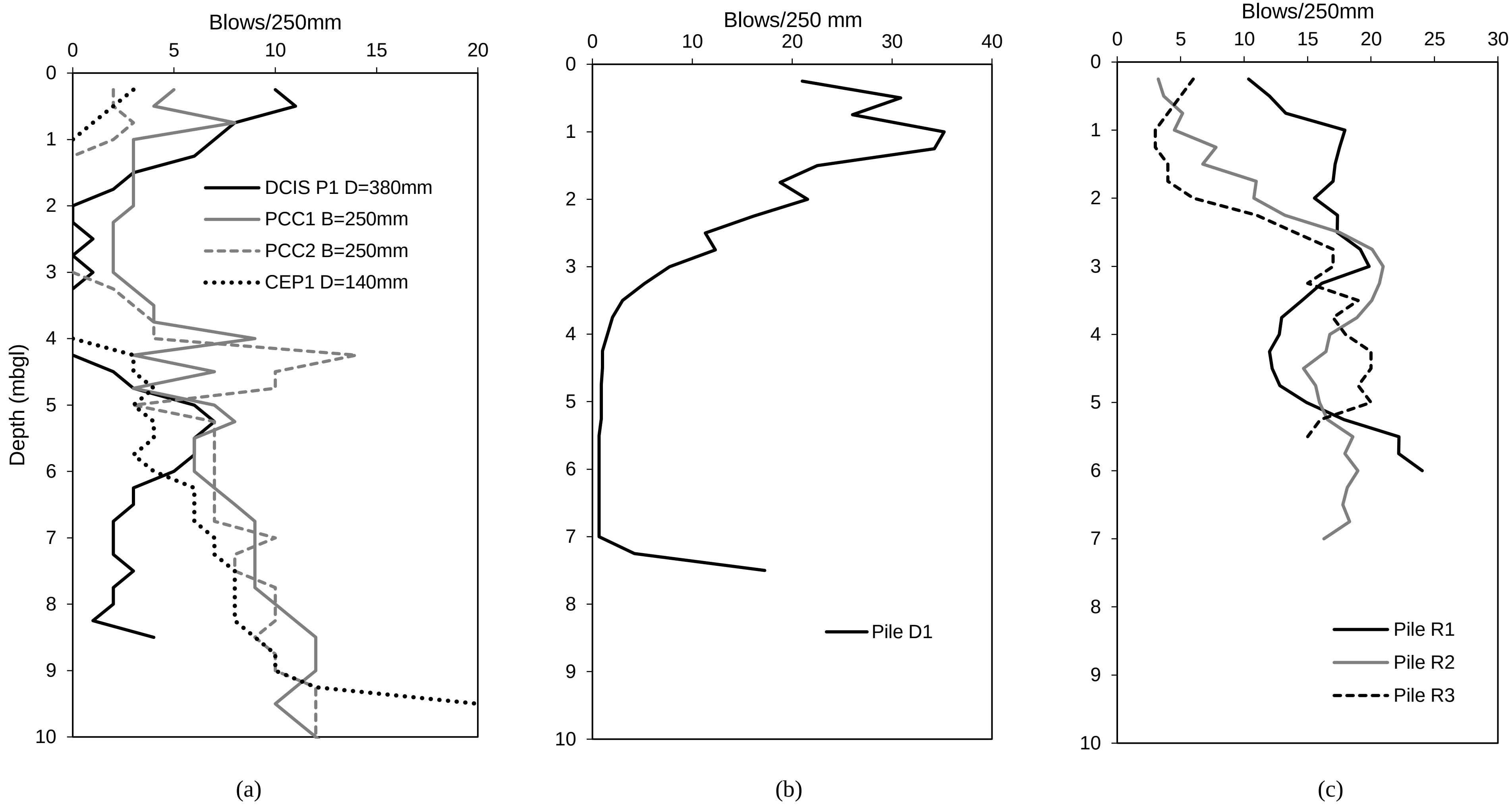

Fig. 6. Driving records at (a) Pontarddulais, (b) Dagenham and (c) Ryton-on-Dunsmore.

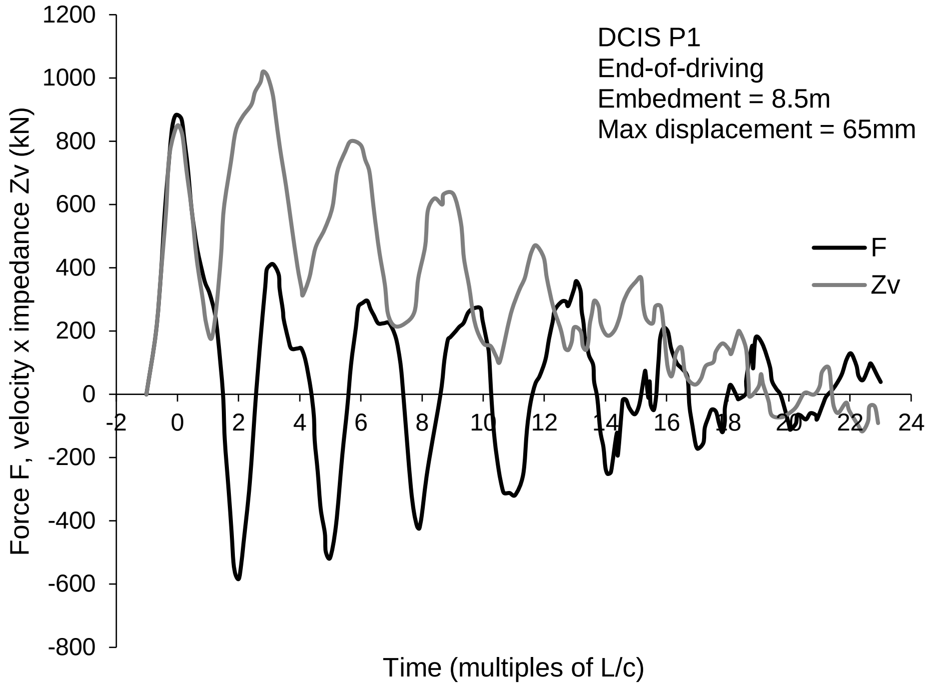

(a)

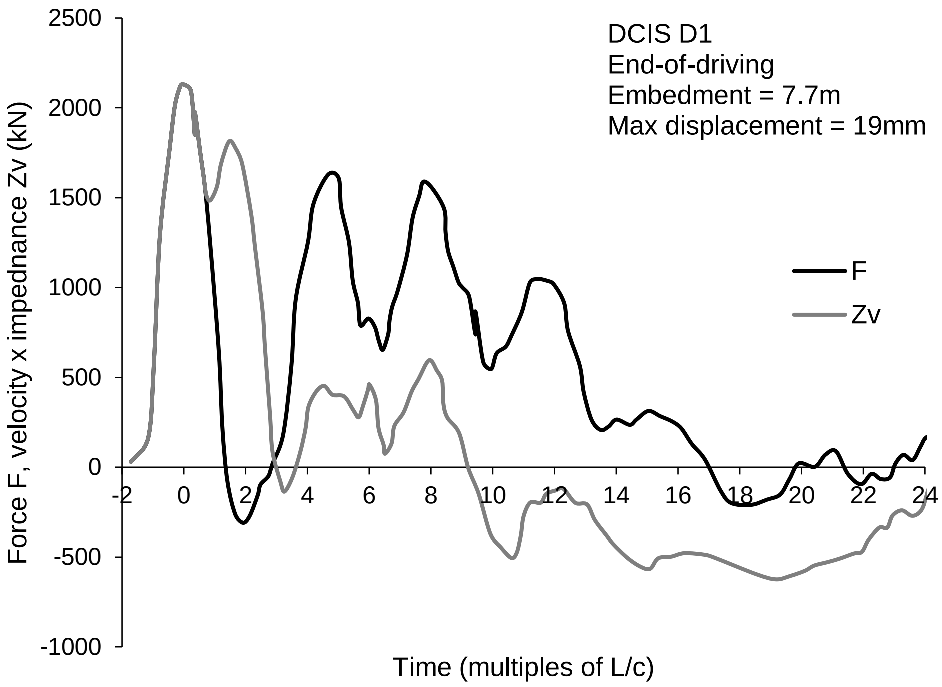

(b)

Fig. 7. Dynamic load test results at end-of-driving of DCIS test piles (a) Pontarddulais and (b) Dagenham

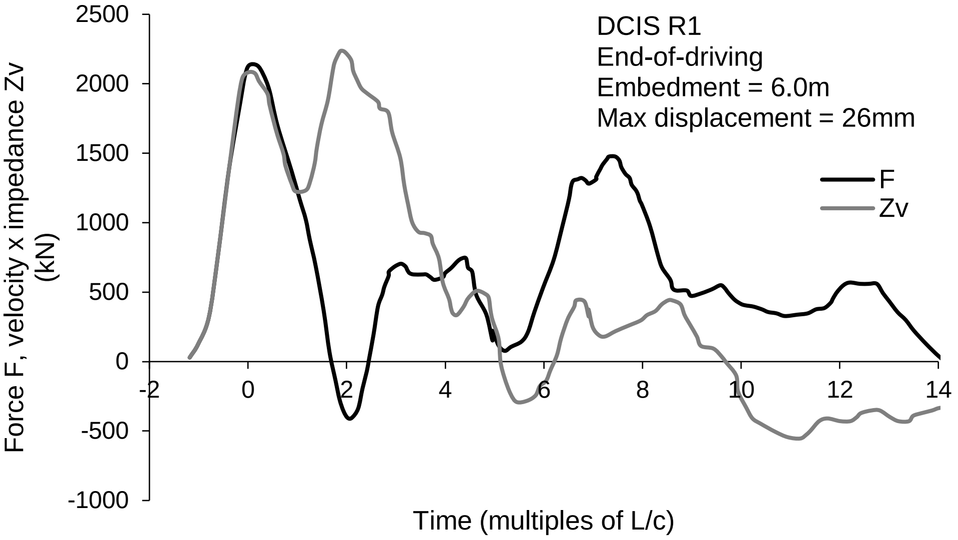

(a)

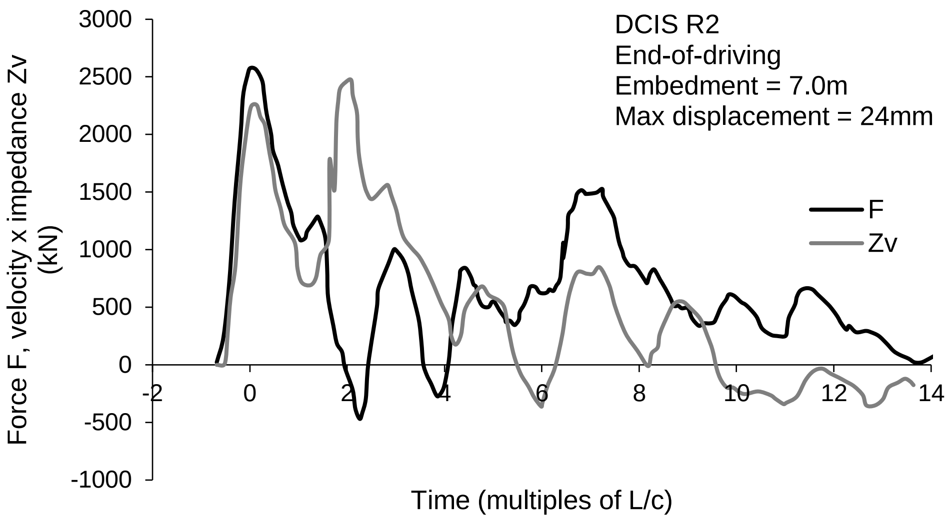

(b)

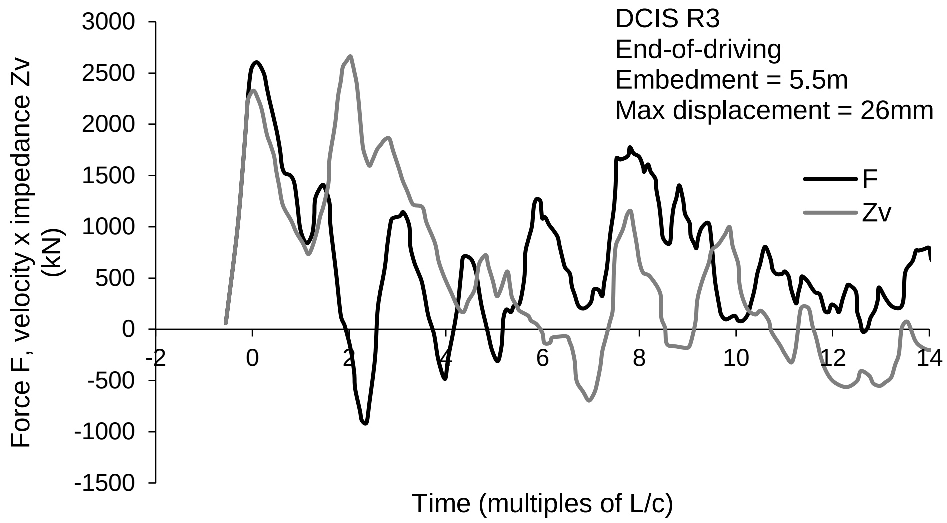

(c)

Fig. 8. Dynamic load test results at end-of-driving of DCIS test piles (a) R1, (b) R2 and (c) R3 at Ryton-on-Dunsmore

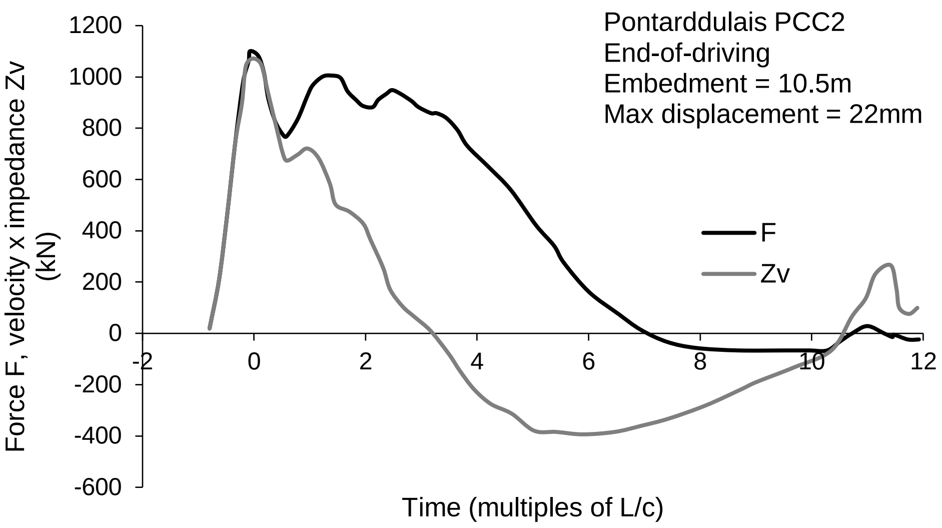

(a)

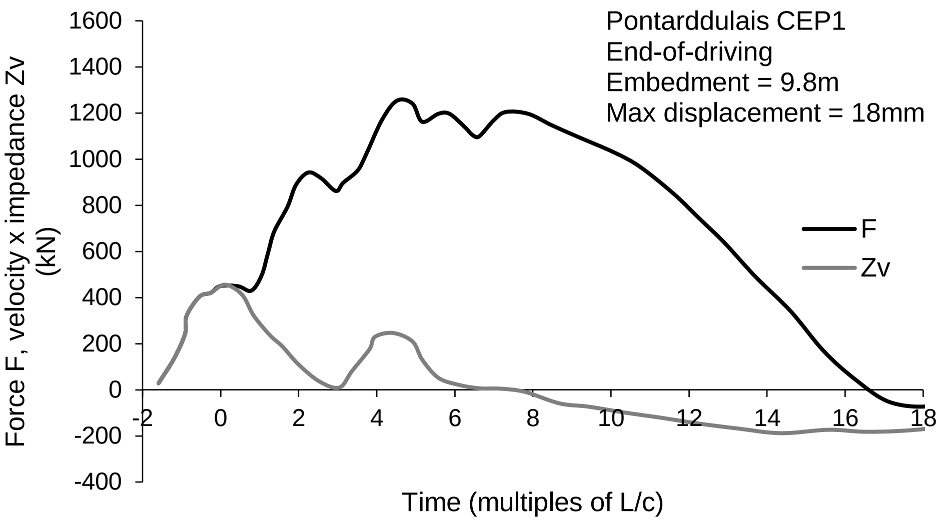

(b)

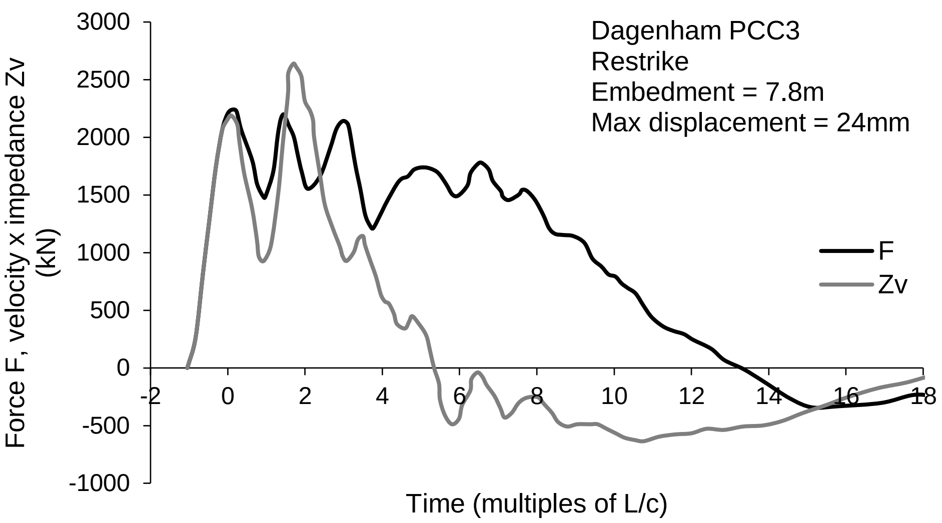

(c)

Fig. 9. Dynamic load test results (a) precast pile PCC2 at Pontarddulais, (b) closed-ended steel pile CEP1 at Pontarddulais and (c) precast pile at PCC3 at Dagenham.

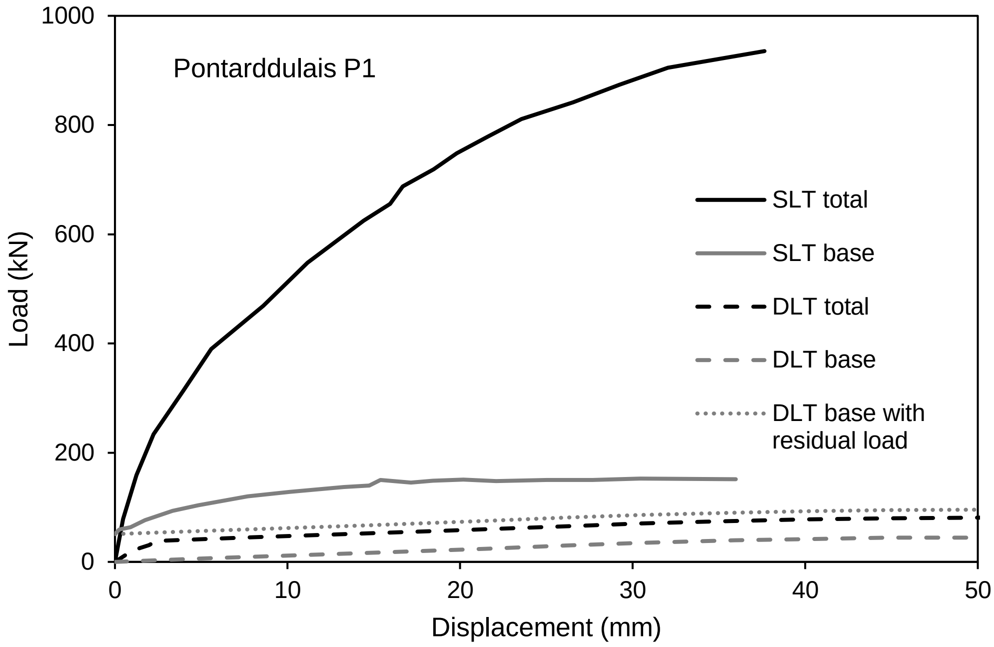

(a)

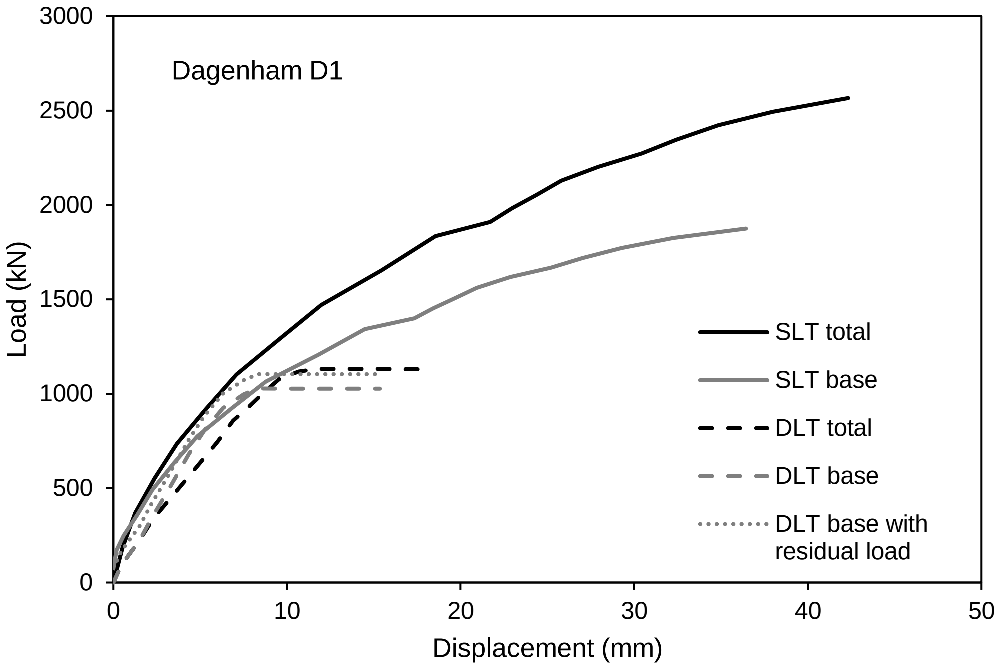

(b)

Fig. 10. Test pile load-displacement curves at (a) Pontarddulais and (b) Dagenham

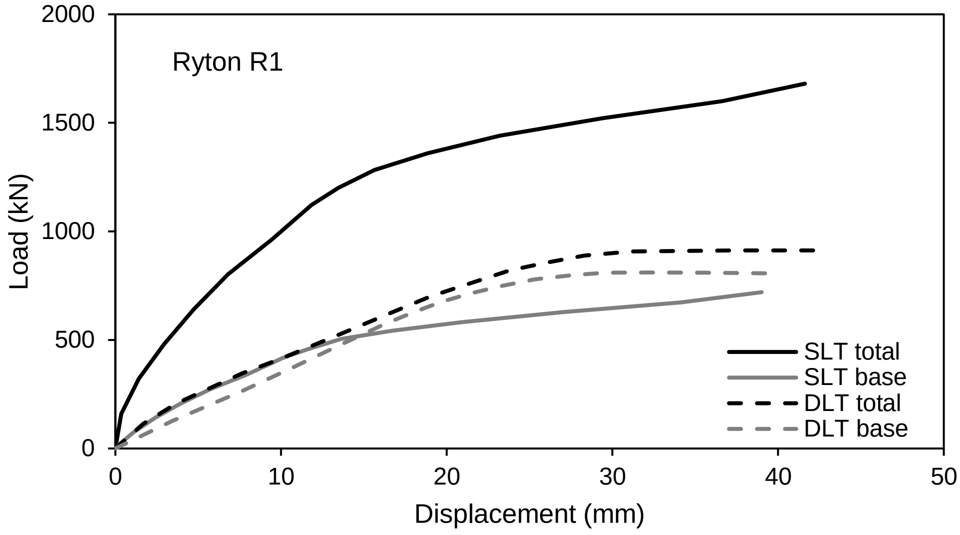

(a)

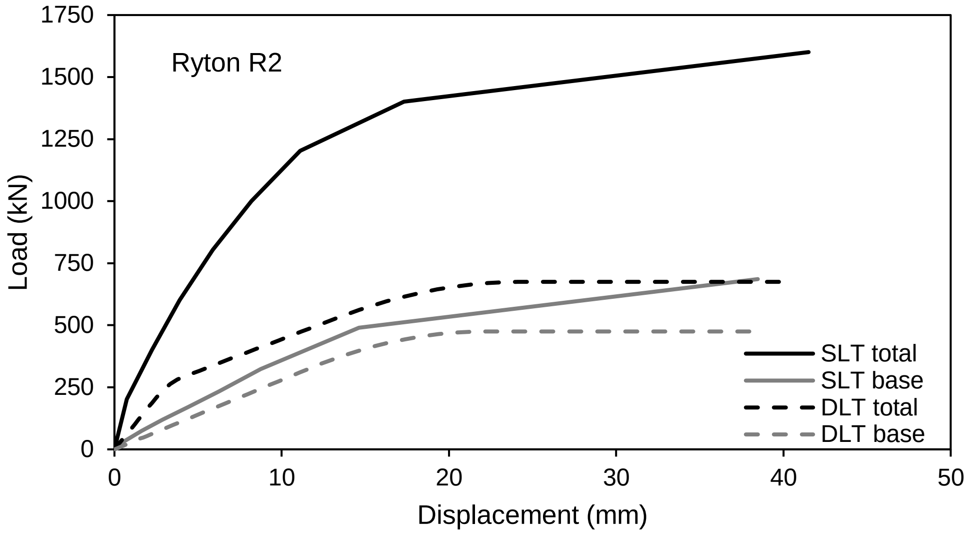

(b)

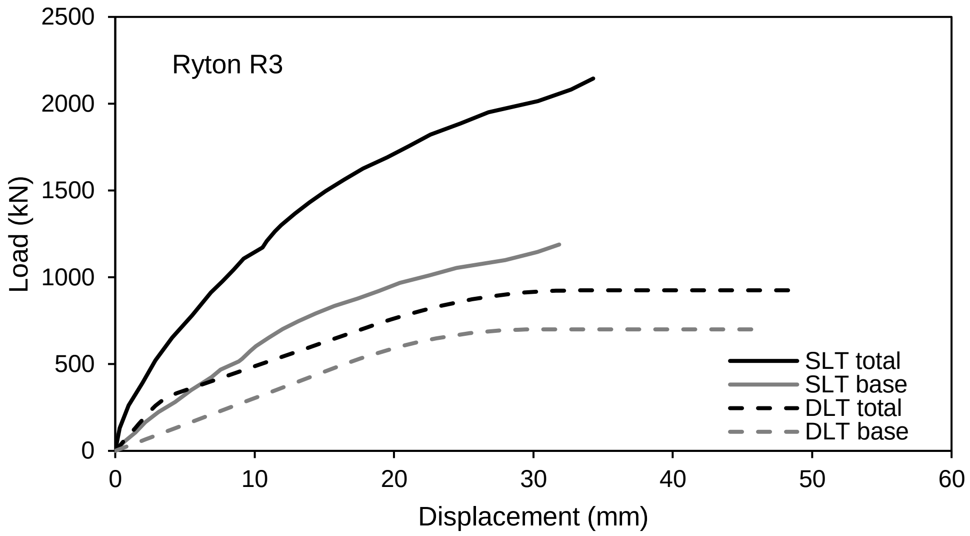

(c)

Fig. 11. Test pile load-displacement curves at Ryton-on-Dunsmore for (a) Pile R1, (b) Pile R2 and (c) Pile R3.

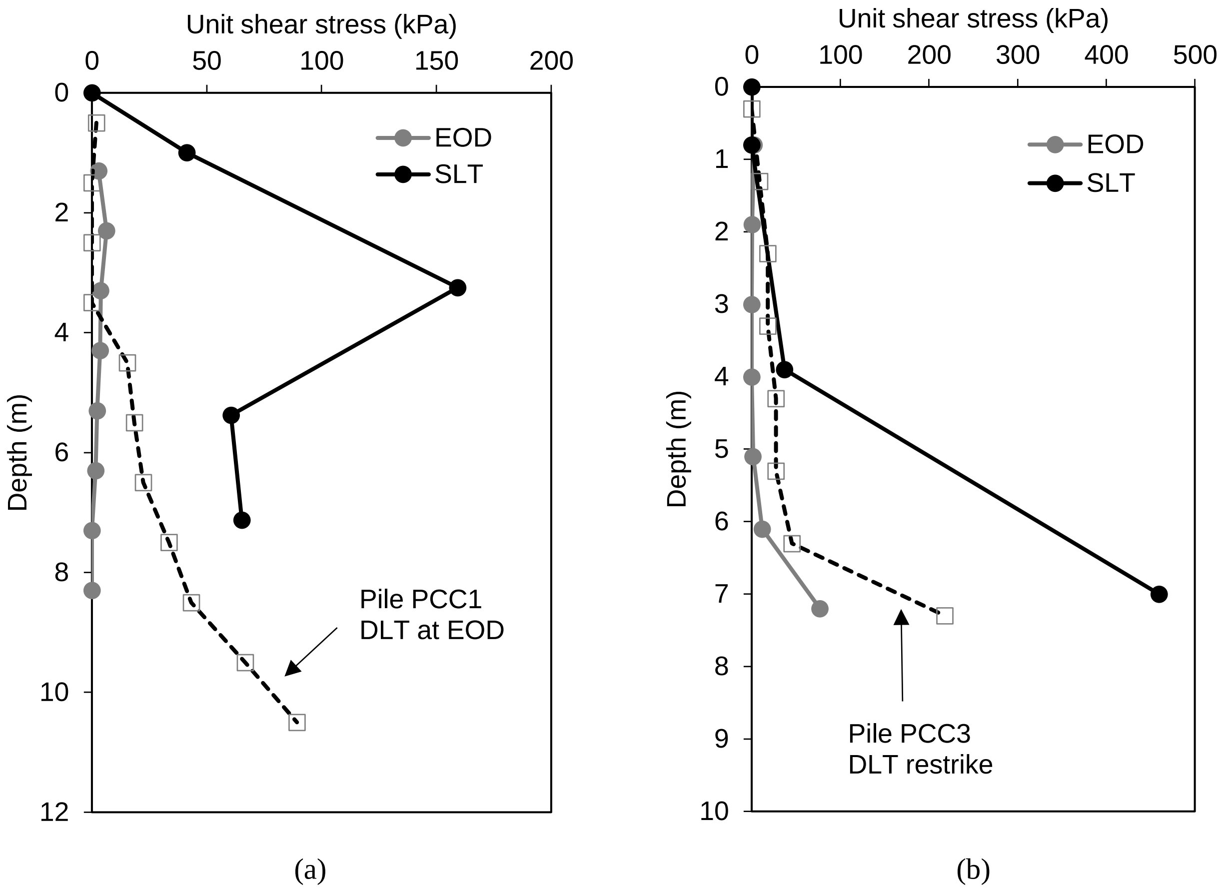

Fig. 12. Variation in mobilised unit shear stress with depth at (a) Pontarddulais and (b) Dagenham.

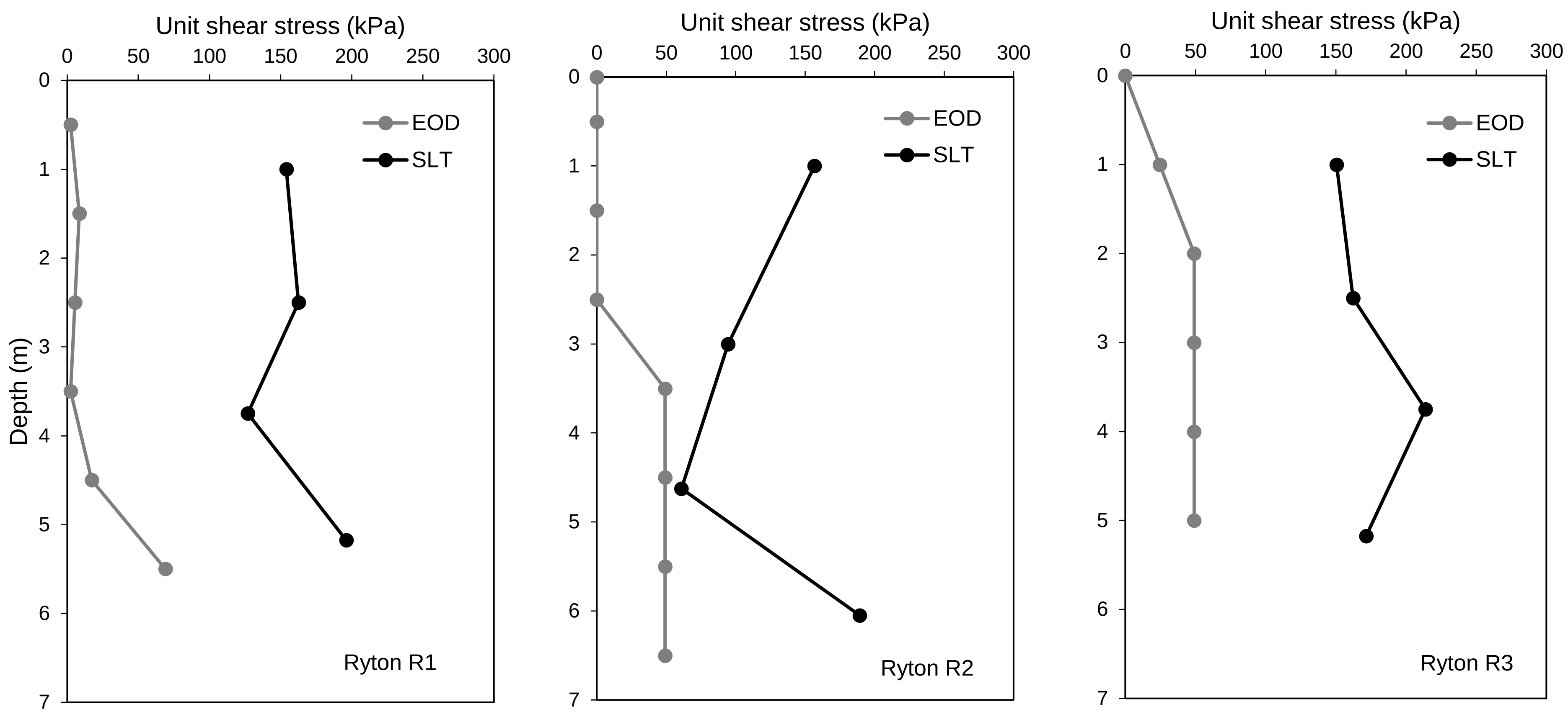

(a) (b) (c)

Fig. 13. Variation in mobilised unit shear stress with depth at Ryton-on-Dunsmore for (a) Pile R1, (b) Pile R2 and (c) Pile R3.

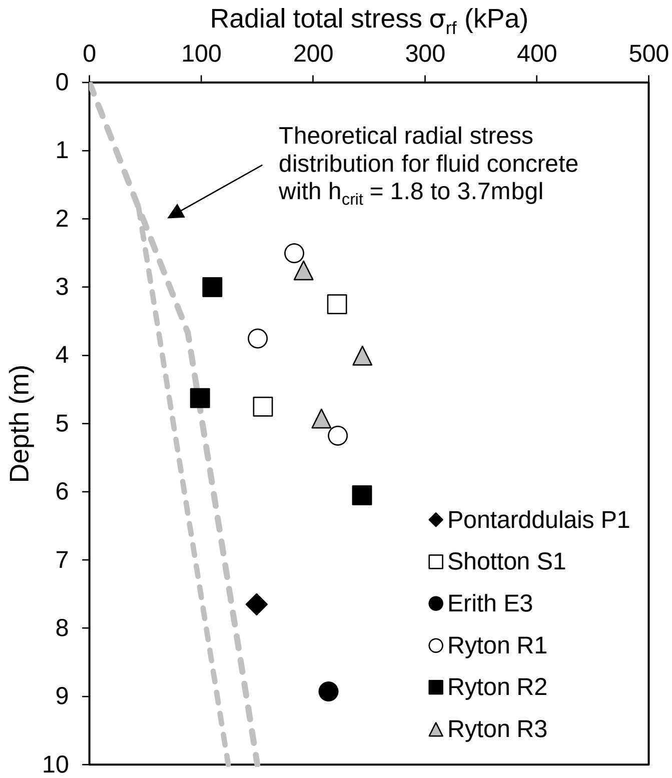

Fig. 14. Comparison of inferred radial total stress and fluid concrete pressure with depth for DCIS piles.

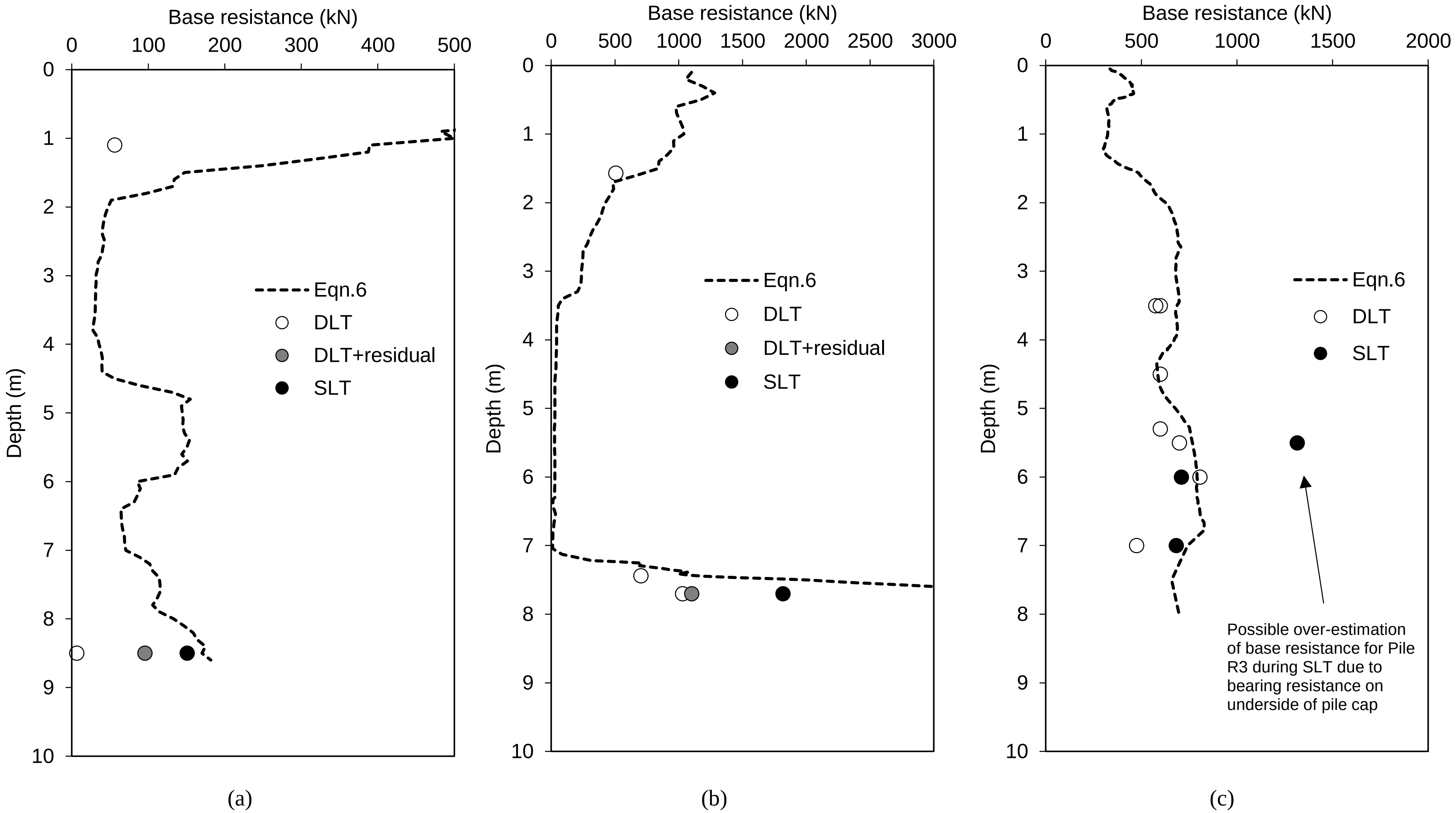

Fig. 15. Comparison of mobilised base resistance for dynamic and static load tests with predicted base resistance using Equation 6 at (a) Pontarddulais, (b) Dagenham and (c) Ryton-on-Dunsmore

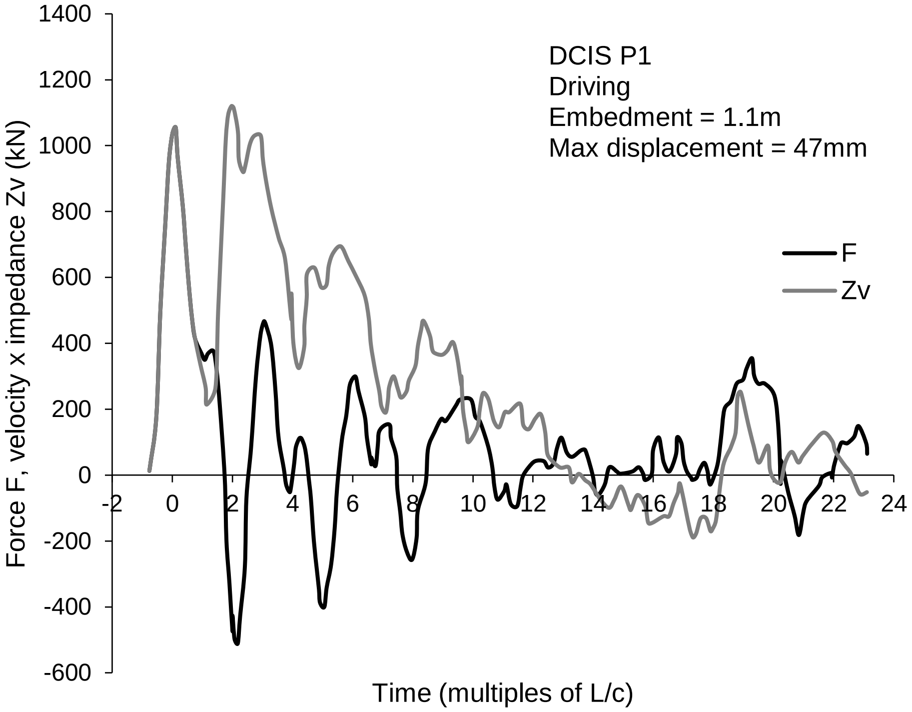

Figure S1: Dynamic load test results for Pile P1 during driving at 1.1mbgl

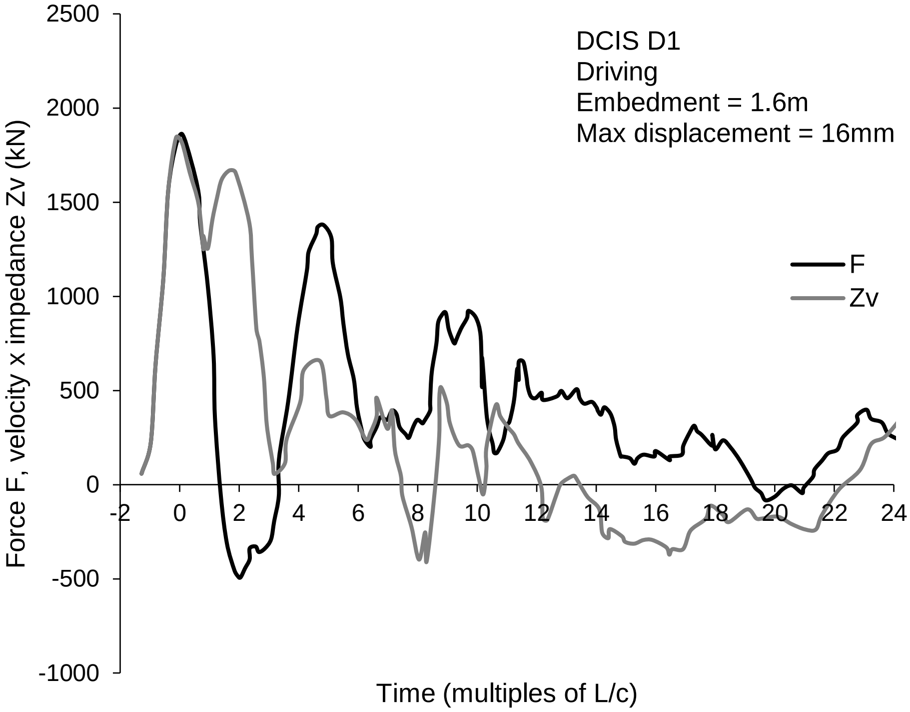

Figure S2: Dynamic load test results for Pile D1 during driving at 1.6mbgl

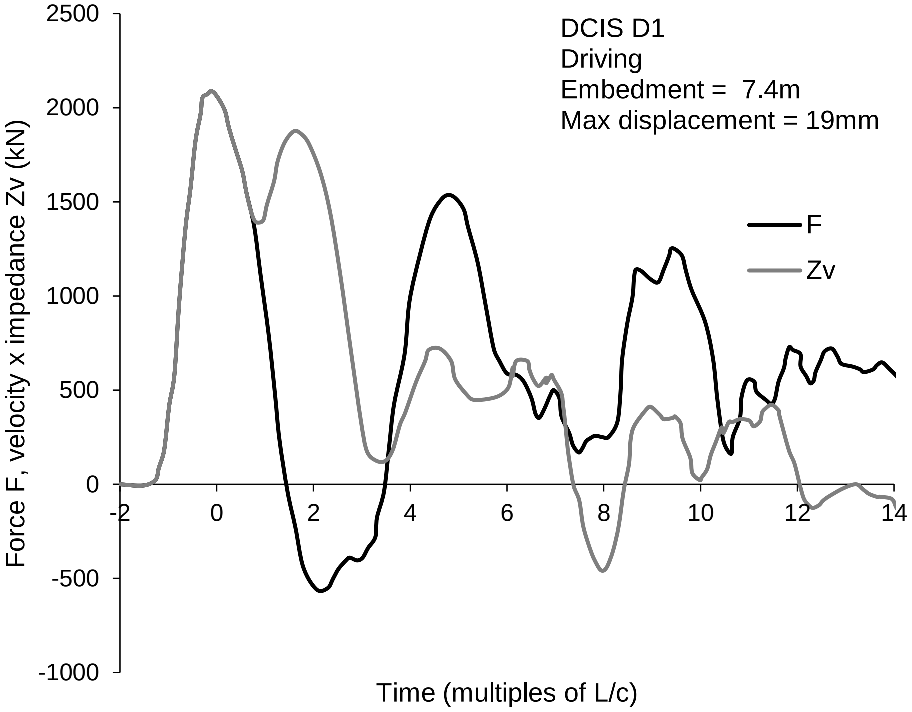

Figure S3: Dynamic load test results for Pile D1 during driving at 7.4mbgl

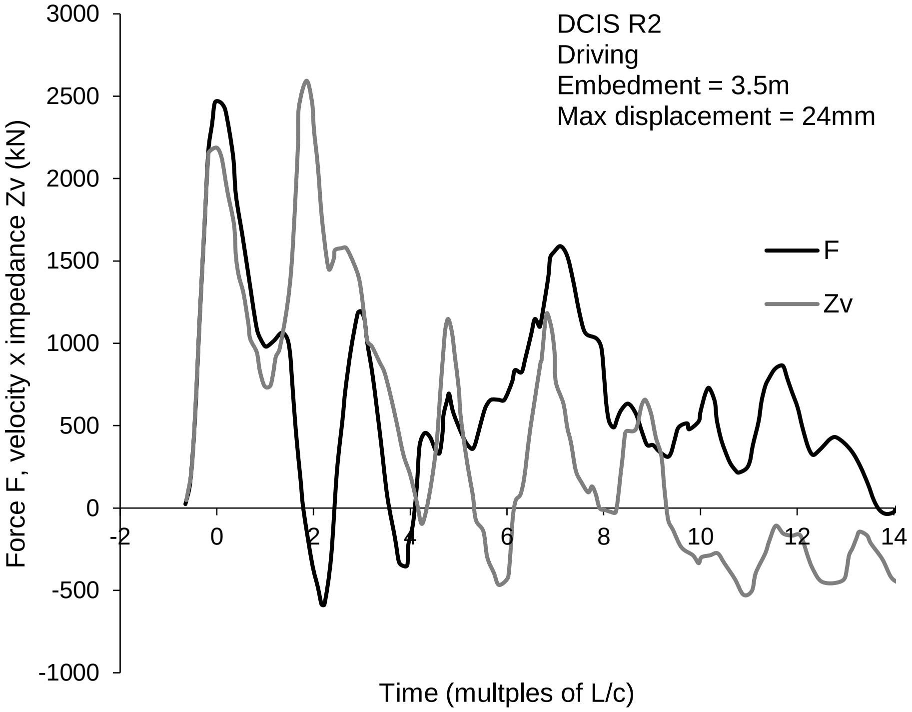

Figure S4: Dynamic load test results for Pile R2 during driving at 3.5mbgl

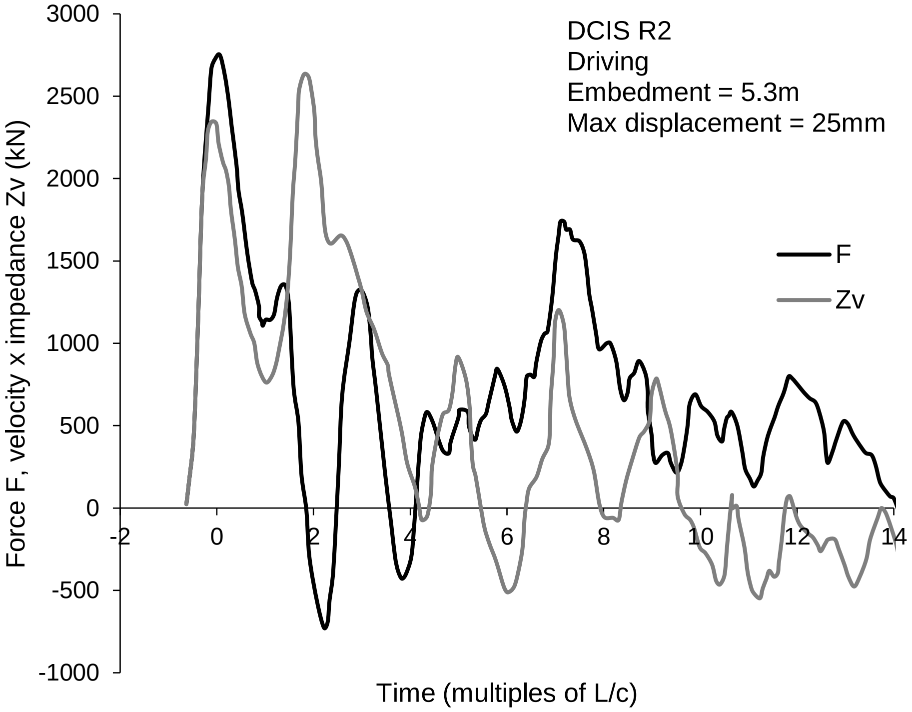

Figure S5: Dynamic load test results for Pile R2 during driving at 5.3mbgl

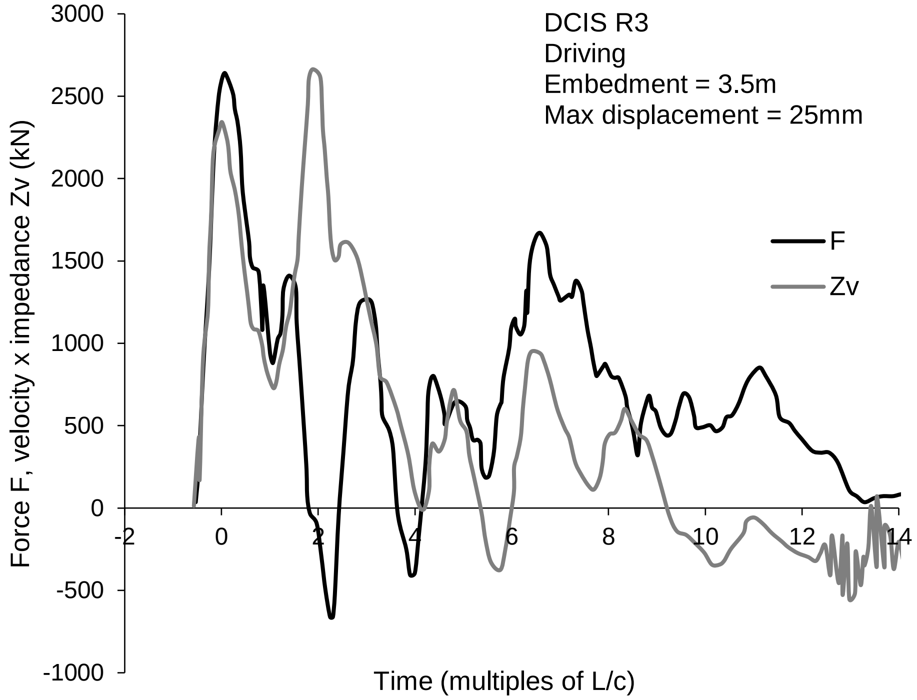

Figure S6: Dynamic load test results for Pile R3 during driving at 3.5mbgl

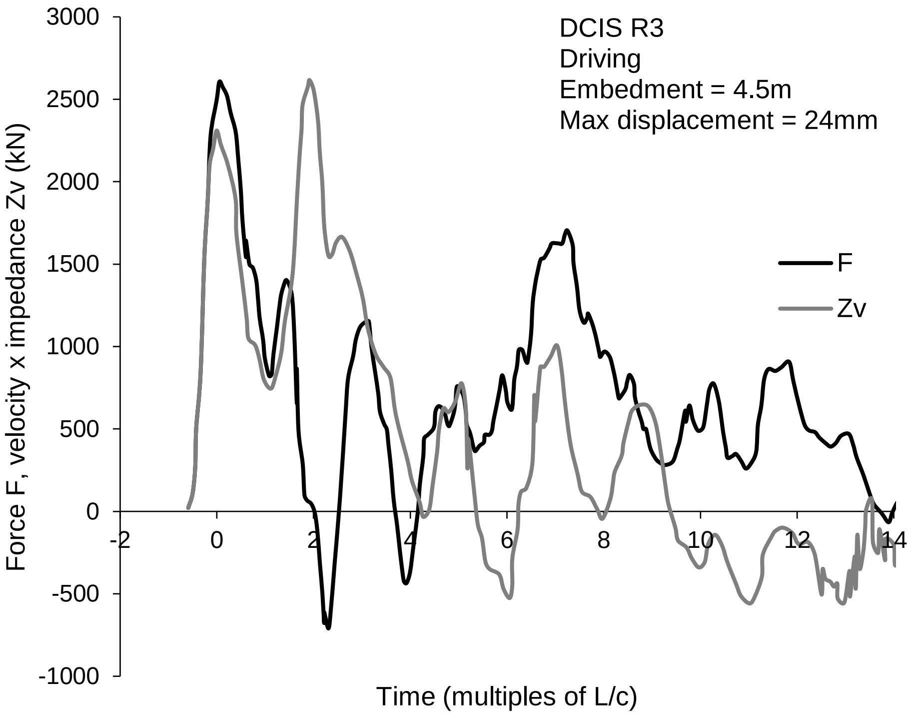

Figure S7: Dynamic load test results for Pile R3 during driving at 4.5mbgl